JBC RESEARCH ARTICLE

The adapter protein FADD provides an alternate pathway for entry into the cell cycle by regulating APC/C-Cdh1 E3 ubiquitin ligase activity

Received for publication, February 20, 2023, and in revised form, April 11, 2023 Published, Papers in Press, May 4, 2023,
https://doi.org/10.1016/j.jbc.2023.104786

Sahezeel Awadia[1], Merna Sitto[1], Sundaresh Ram[2], Wenbin Ji[1], Yajing Liu[1], Raheema Damani[3], Dipankar Ray[1], Theodore S. Lawrence[1], Craig J. Galban[2], Steven D. Cappell[4], and Alnawaz Rehemtulla[1,*]

From the [1]Department of Radiation Oncology, and [2]Department of Radiology and Biomedical Engineering, University of Michigan Medical School, Ann Arbor, Michigan, USA; [3]Department of Biomedical Engineering, University of Alabama, Birmingham, Alabama, USA; [4]Laboratory of Cancer Biology and Genetics, Center for Cancer Research, National Cancer Institute, Bethesda, Maryland, USA

Reviewed by members of the JBC Editorial Board. Edited by Donita Brady

The E3 ubiquitin ligase APC/C-Cdh1 maintains the G0/G1 state, and its inactivation is required for cell cycle entry. We reveal a novel role for Fas-associated protein with death domain (FADD) in the cell cycle through its function as an inhibitor of APC/C-Cdh1. Using real-time, single-cell imaging of live cells combined with biochemical analysis, we demonstrate that APC/C-Cdh1 hyperactivity in FADD-deficient cells leads to a G1 arrest despite persistent mitogenic signaling through oncogenic EGFR/KRAS. We further show that $FADD_{WT}$ interacts with Cdh1, while a mutant lacking a consensus KEN-box motif ($FADD_{KEN}$) fails to interact with Cdh1 and results in a G1 arrest due to its inability to inhibit APC/C-Cdh1. Additionally, enhanced expression of $FADD_{WT}$ but not $FADD_{KEN}$, in cells arrested in G1 upon CDK4/6 inhibition, leads to APC/C-Cdh1 inactivation and entry into the cell cycle in the absence of retinoblastoma protein phosphorylation. FADD's function in the cell cycle requires its phosphorylation by CK1α at Ser-194 which promotes its nuclear translocation. Overall, FADD provides a CDK4/6-Rb-E2F-independent "bypass" mechanism for cell cycle entry and thus a therapeutic opportunity for CDK4/6 inhibitor resistance.

Cell division is a tightly regulated process to ensure the production of two genetically identical cells and is often dysregulated in cancer, wherein oncogenic mutations perturb the cell cycle leading to uncontrolled cell division. The somatic mammalian cell cycle involves a tightly regulated, precise, and sequential phase transition through G1, S, G2, and M. Entry into the cell cycle requires the activation of G1 cyclin-dependent kinases (CDK4/6), which inactivates the retinoblastoma protein (Rb) by its phosphorylation (1, 2). Inactive Rb releases the E2F transcription factor from inhibition leading to the transcription of E2F targets including cyclin E and early mitotic inhibitor 1 (Emi1) (3, 4). Ubiquitination of S-phase cyclins (*e.g.*, cyclin A2 and cyclin E) and Emi1 (3, 5–7), by the E3 ligase, Anaphase Promoting Complex with its co-activator Cdh1 (APC/C-Cdh1) and subsequent degradation by the proteasomal machinery provides a strict unidirectional behavior of the cell cycle, necessitating inactivation of the APC/C-Cdh1 prior to entry into the cell cycle (8, 9). Accumulation of cyclin E leads to activation of the cyclin-dependent kinase CDK2, which in collaboration with Emi1 provides a feed-forward loop for APC/C-Cdh1 inactivation, a critical decision point, required for a rapid and robust accumulation of S-phase cyclins triggering the transition of cells into S phase and an irreversible commitment to proliferate (3, 8, 10–16).

Fas-associated protein with death domain (FADD) was originally identified as an adapter for death receptor-mediated activation of the extrinsic apoptosis cascade (17–19). However, recent evidence has also ascribed a non-apoptotic function of FADD in cell proliferation, wherein the increased abundance of FADD, specifically that of the phosphorylated, nuclear-localized form, is predictive of aggressive disease and poor clinical outcome in patients with lung adenocarcinoma (20–22). Amplification of the *FADD* locus on chromosome 11q13.3 is frequently observed in human cancers (23–26). Using conditional, genetically engineered mouse models of lung cancer, we have previously demonstrated a requirement for FADD and its phosphorylation at Serine-194 for mutant KRAS-mediated oncogenic transformation in lung cancer (22). However, the mechanistic underpinning for FADD's non-apoptotic function in oncogenesis remains to be elucidated.

Findings presented here reveal that FADD promotes entry into the cell cycle and the G1 to S cell cycle transition. Analogous to Emi1, the association of FADD with Cdh1 leads to the inhibition of APC/C-Cdh1 E3 ligase activity which is required for the G1 to S transition. A consensus KEN-box domain (27) within the C-terminus of FADD was found to be necessary for interaction with Cdh1 and the inactivation of APC/C-Cdh1. The significance of FADD in cell cycle entry was demonstrated by its ability to promote G1 to S transition in the absence of cyclin D/CDK4/6 activity and Rb phosphorylation. In summary, these findings demonstrate a role for FADD as an alternate pathway for APC/C-Cdh1 inactivation and therefore

* For correspondence: Alnawaz Rehemtulla, alnawaz@umich.edu.

entry into the cell cycle as well as a new understanding of the role of a pro-apoptotic protein FADD in promoting cell proliferation, consistent with our previous finding that elevated FADD levels correlate with poor clinical outcomes in patients with lung cancer (21).

Results

FADD is required for G1 to S transition in mutant EGFR lung adenocarcinoma cells

In an effort to quantitatively evaluate the role of FADD in the transition through each phase of the cell cycle at high temporal resolution, we utilized time-lapse live cell imaging using the PIP-FUCCI reporter (28). PIP-FUCCI consists of a Cdt1 degron fused to the mVenus fluorescent tag as well as a Geminin degron fused to the mCherry tag (Fig. 1*A*, top). Cdt1 is stable during G1 and degraded rapidly upon entry into the S phase, while Geminin is ubiquitylated and degraded from anaphase through G1 by APC/C-Cdh1 but accumulates upon entry into the S phase. Hence, mCherry accumulation (APC/C-Cdh1 inactivation) and mVenus degradation serve as surrogates for quantitative and precise evaluation of the G1 to S transition (APC/C-Cdh1 inactivation) (Fig. 1*A*, bottom). We generated stable cell lines expressing PIP-FUCCI and performed live cell imaging. Analysis of fluorescence images revealed Cdt1-mVenus stabilization (green nuclei) and Geminin-mCherry degradation (loss of red fluorescence) immediately following mitosis (Fig. 1, *A* and *B*), persisted for 8 h, followed by a rapid decrease in Cdt1-mVenus fluorescence and a corresponding accumulation in Geminin-mCherry fluorescence, indicative of a transition into the S phase from G1 (single cell nuclei shown in Fig. 1*B*). At 20 h post-mitosis, accumulation of Cdt1-mVenus, simultaneous with peak Geminin-mCherry fluorescence, is indicative of G2/M phase of the cell cycle. A rapid decrease in Geminin-mCherry fluorescence was observed upon mitosis and daughter cell production after 24 h to reinitiate the cell cycle (Fig. 1*B*).

EGFR, a transmembrane receptor tyrosine kinase, is often overexpressed or mutated in lung cancer. NCI-H1975 lung adenocarcinoma cells harbor a mutation in EGFR (L858 R) that stabilizes the active dimeric form of the receptor thus driving uncontrolled cell proliferation as well as a T790M mutation that is associated with resistance to first-generation EGFR inhibitors (29, 30). HCC827 lung cancer cells express a constitutively active mutant EGFR (exon 19 deletion) (31) (Fig. 1*C*). To understand the role of FADD in the cell cycle using EGFR-driven cancer cells, we performed siRNA-mediated knockdown of FADD using two independent target sequences (Fig. S1*A*). In contrast to control NCI-H1975 cells, FADD-depleted cells showed a persistent Cdt1-mVenus fluorescence following mitosis wherein accumulation of Geminin-mCherry fluorescence (G1 to S transition) was not observed in 60% of the cells for the entire imaging period (>40 h, Fig. 1*D*) Interestingly, some cells (Fig. 1*D*, lower panel, FADD KD) did undergo a G1 to S transition which was delayed to 24 h (compared to 8–10 h for control). To rule out the possibility that the observed defect in the G1 to S transition in FADD KD cells was due to a defect prior to entry into G1, we evaluated the time in S and G2/M during the previous cycle. Compared to control cells, FADD-depleted cells did not show an obvious alteration of the time in S or G2/M (8 h and 6 h respectively), while the subsequent mean time in G1 was extended from 8 h to 24 h in FADD-depleted cells compared to the control siRNA treated cells (Fig. 1*E*). Single-cell traces of the PIP-FUCCI reporter for the S and G2/M phases in FADD-depleted and control NCI-H1975 cells are shown in Fig. S1*B*, revealing that the S and G2/M of G1 protracted cells were unaltered compared to control siRNA-treated cells. Quantitative evaluation of cells arrested in G1 at 48 h post-transfection revealed that almost 60% of FADD-depleted cells (FADD KD) were arrested, in contrast to none in the control siRNA-treated cells (CTRL) (Fig. 1*F*). Analysis of mitotic events per 100 cells over a 48 h period revealed that 100% of control cells underwent at least one round of mitosis, whereas only 5% of FADD siRNA treated cells underwent mitosis indicating that FADD-depleted cells demonstrate defective G1 to S transition. (Fig. 1*G*). The defect in the G1 to S transition upon FADD depletion was recapitulated in an independent lung cancer cell line having constitutive EGFR mitogenic signaling wherein a protracted G1 or a G1 arrest, as well as fewer mitotic events, were observed (HCC827, Fig. S2, *A*–*C*).

A delay in Geminin-mCherry accumulation in FADD-depleted cells suggested a defect in timely APC/C-Cdh1 inactivation (and hence a defect in G1 to S transition). To evaluate this biochemically, we synchronized NCI-H1975 cells at G2/M using a Cdk1 inhibitor, CDK1i (RO-3306). Upon release, cells were collected at various times to evaluate the degradation and accumulation of APC/C-Cdh1 substrates. In control cells, cyclin B1, cyclin A2, and Securin were observed at peak levels immediately upon release from CDK1i, when APC/C-Cdh1 is inactive (G2/M, Fig. 1*H*, CTRL, 0 h), and degraded at 8 h, when APC/C-Cdh1 is reactivated upon mitotic exit (confirmed by peak phospho-Histone H3). Re-accumulation of cyclin B1, cyclin A2, and Securin levels at 24 h post CDK1i release in control cells is consistent with APC/C-Cdh1 inactivation and entry into S from G1. In contrast, FADD-depleted cells failed to show an accumulation of cyclin B1, cyclin A2, or Securin at the expected time (Fig. 1*H*, right panel (FADD KD)). Quantitative analysis of cyclin B1 and cyclin A2 levels in replicate experiments (Fig. 1*I*) confirmed a defect in the accumulation of APC/C-Cdh1 substrates in the absence of FADD. In aggregate, these results demonstrate that FADD depletion in EGFR-driven NCI-H1975 and HCC827 lung adenocarcinoma cells results in a defect in the G1 to S transition, likely due to a failure to inactivate APC/C-Cdh1.

FADD is required for G1 to S transition in KRAS mutant lung cancer cells

KRAS is a component of the RAS/MAPK signaling pathway that relays mitogenic signals to the nucleus upon cell surface receptor activation (including EGFR). KRAS is a GTPase, which switches from its inactive GDP-bound form to an active

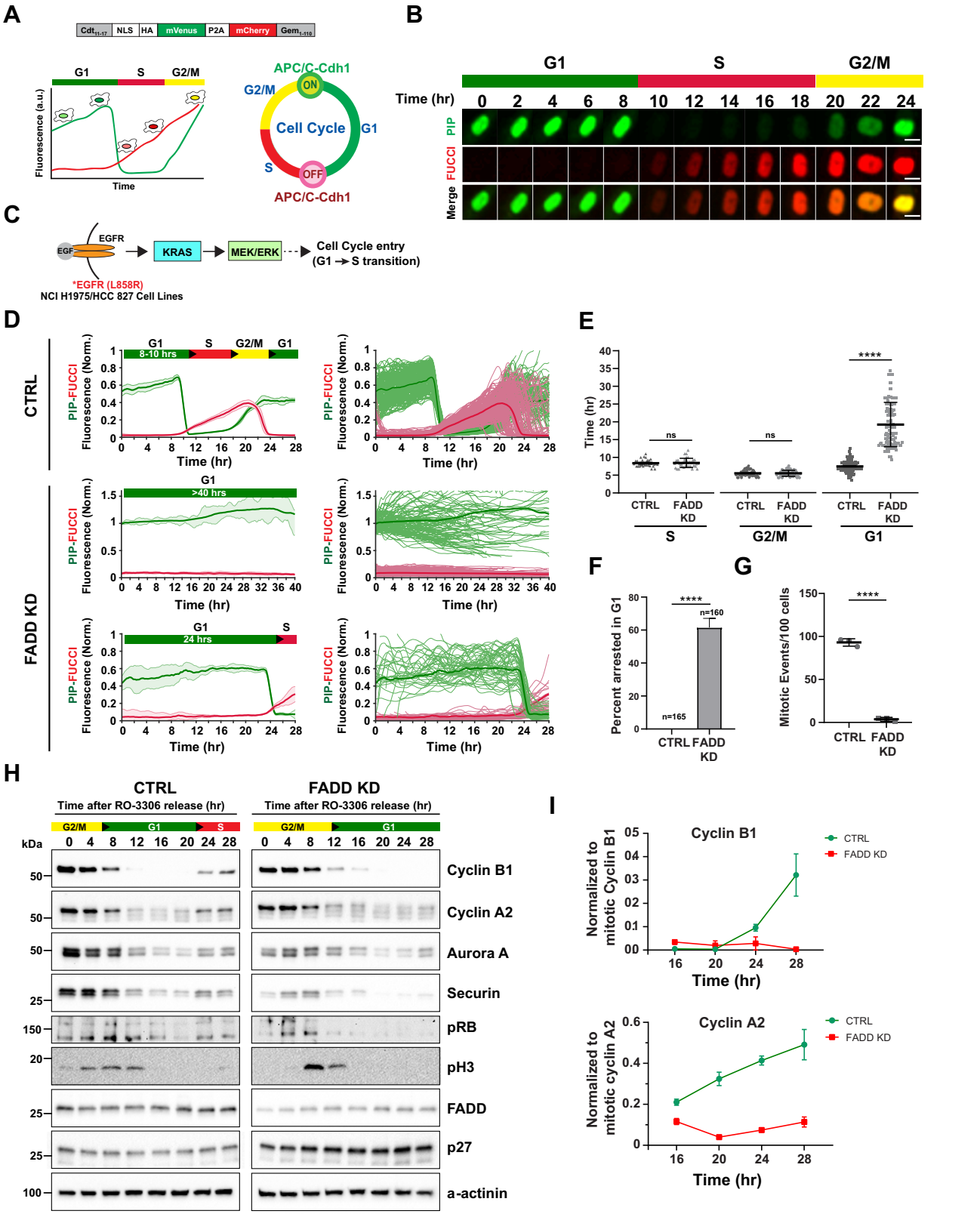

Figure 1. FADD is required for efficient cell cycle entry in lung cancer cells having oncogenic EGFR. *A*, the PIP-FUCCI dual reporter expression construct. The PIP-Cdt1 polypeptide consists of the $Cdt1_{1–17}$ PIP (PCNA-interacting protein) degron and an NLS fused to mVenus. The $Gem_{1–110}$ polypeptide consists of the D-box and the KEN-box degron motifs of Geminin fused to mCherry. The P2 self-cleaving peptide separates the two fluorescent polypeptides (*top panel*). The PIP-FUCCI cell cycle reporter is designed such that during G1, the Cdt1-mVenus polypeptide is stable, while the Geminin-mCherry polypeptide is degraded (APC/C-Cdh1 is activated) and hence cells demonstrate green fluorescence. Upon entry into S phase, inactivation of APC/C-Cdh1 results in stabilization of geminin-mCherry but degradation of Cdt1-mVenus resulting in *red* fluorescence. In the G2 phase, both polypeptides are stable and hence cell fluoresce yellow (*green* + *red*) (*lower panel*). A schematic of cell cycle transitions emphasizing APC/C-Cdh1 inactivation prior to entry into S phase and that APC/C-Cdh1 activity is characteristic of cells in G1. *B*, images of a single nucleus from confocal time-lapse imaging of stable PIP-FUCCI reporter

GTP-bound form upon receptor activation. Mutated RAS oncoproteins (15–25% of lung adenocarcinoma) differ functionally from their normal counterparts in that they remain in a GTP-bound active state, which constitutively signals through the RAS/MAPK pathway, activating a transcriptional program that promotes uncontrolled cell proliferation as a result of uncontrolled cell cycle entry (Fig. 2*A*) (32). To investigate if FADD also participates in the G1 to S transition in lung cancer cells harboring mutant KRAS, we utilized NCI-H441 cells expressing stable PIP-FUCCI reporter. Control NCI-H441 cells exhibit high Cdt1-mVenus levels upon mitosis and low Geminin-mCherry levels indicative of active APC/C-Cdh1 (Fig. 2*B*, CTRL). Knockdown of FADD resulted in a delayed G1 to S transition which required 20 h (compared to 10 h in control cells) (Fig. 2*B* and *C*). These studies revealed that the time in S or G2/M in cells that experienced a delayed G1 to S transition was not significantly altered (Fig. 2*C*) and that the cell cycle defect could be attributed to a delayed G1 to S transition or a G1 arrest in 30% of the cells (Fig. 2*D*). Live cell traces of the PIP-FUCCI reporter used to derive these results shown in Fig. S3*A*, demonstrate that individual cells which experience a G1 arrest in the absence of FADD had an unaltered S and G2/M when compared to CTRL. Quantitative analysis of mitotic events revealed that only 10% of FADD-depleted cells underwent mitosis during the 48 h experiment compared to 100% of the control cells (Fig. 2*E*). To biochemically demonstrate that the delay in G1 to S transition observed in NCI-H441 cells is due to APC/C-Cdh1 hyperactivity in FADD-depleted cells, we conducted a synchronization experiment as above in Figure 1*H*. In contrast to non-synchronized cells (NS, Fig. 2*F*) G2/M arrested cells demonstrated peak cyclin B1, cyclin A2, Securin, and Aurora A levels in the presence of nocodazole (G2/M arrested cells, NOC, Fig. 2*F*) and CDK1i (0 h, Fig. 2*F*, CTRL). Upon mitosis and entry into G1, a decrease in levels of each of the above APC/C-Cdh1 substrates was observed at 4 h, demonstrating activation of the APC/C-Cdh1. Subsequent entry into the S phase at 20 h in control cells was marked by an accumulation of each of these APC/C substrates indicative of APC/C-Cdh1 inactivation (Fig. 2*F*, CTRL). In cells having FADD knockdown, although peak levels of cyclin B1, cyclin A2 and Aurora A (in G2/M) were observed upon release from CDK1i at the expected time (0 and 4 h, Fig. 2*F*, FADD KD); however, a transition from G1 into S was not observed as the levels of cyclin B1, cyclin A2, Aurora A, and Securin failed to accumulate to the levels observed in control cells as quantified using replicate experiments (Fig. 2*G*). A failure to accumulate each of these APC/C-Cdh1 degron-containing proteins is consistent with a failure to inactivate APC/C-Cdh1 at the expected time in FADD-depleted cells. Interestingly, analysis of NCI-H441 cells (Fig. 2*F*) also revealed that FADD levels were highest in G2/M and decreased precipitously at the end of mitosis and began to reaccumulate prior to entry into the S phase from G1 suggesting that FADD may also be regulated in a cell cycle phase-dependent manner. A similar but less pronounced fluctuation of FADD levels in a cell cycle phase-dependent manner was also observed in NCI-H1975 cells (Fig. 1*H*). In NCI-H441 cells, expression of Emi1, a well-appreciated regulator of the G1/S transition, was not detectable (Fig. S3*B*), although MCF7 cells had readily detectable levels of Emi1 under identical conditions.

To investigate if the observed defect in the G1 to S transition observed in FADD-depleted cells was specific to cancer cells or a specific characteristic of lung cancer cells, we evaluated the impact of FADD depletion in MCF-7 breast cancer cells, which are mitogenically driven in response to hormone receptor signaling. Results presented in Fig. S4*A* recapitulate the finding that FADD depletion results in a defective transition of cells from G1 into S using a non-lung cancer cell line. Next, we isolated non-transformed, mouse embryonic fibroblasts (MEF) from conditional mutant KRAS-expressing mice ($KRAS^{G12D}$). This mouse model also harbors an insertionally inactivated FADD genomic locus, which is complemented by a conditional transgene (lox-stop-lox GFP-FADD) (Fig. S4*B*)

expressing NCI-H1975 cells. Cell cycle transition from G1 to S (*green* to *red*) required 8 to 10 h, S to G2 (*red* to *yellow*) required 8 to 10 h and G2/M required 4 to 6 h. Scale bar is 10 μm. *C*, schematic of EGFR-mediated activation of the KRAS-MEK-ERK mitogenic signaling pathway in NCI-H1975 and HCC827 cells. *D*, live cell imaging of control siRNA (CTRL) and FADD KD NCI-H1975 cells was used to obtain fluorescence emission traces of individual cells. Traces were aligned *in silico* at the G1 to S transition (sharp decrease in Cdt1-mVenus signal and a steady increase in Geminin-mCherry signal). The first panel shows the mean of the median traces (*bold plot*) of three independent experiments with variance shown in a *lighter shade*. Individual fluorescence traces of single cells (Cdt1-mVenus and Geminin-mCherry) are also shown. CTRL cells demonstrated an 8 to 10 h G1 phase, while a majority of FADD KD cells were in G1 during the entire imaging time or were in G1 for 24 h. n = 188 for CTRL and 152 for FADD KD cells. *E*, quantification of average time spent in S, G2/M, and G1 phase by CTRL cells and FADD KD cells reveal that in contrast to a 8 to 10 h G1, FADD KD cells had a G1 time of >20 h whereas there is no difference in previous S phase and G2/M time in CTRL *versus* FADD KD cells. n = 58, n = 35 and n = 123 for S, G2/M and G1 respectively. Quantifications are from three independent experiments. Error bars represents mean ± SEM. *$p < 0.05$; **$p < 0.01$; ***$p < 0.001$ and ****$p < 0.0001$, n.s. = non-significant. *F*, bar graph showing percentage of cells arrested in G1 in CTRL and FADD KD NCI-H1975 cells. 60% of FADD knockdown cells demonstrated an arrested G1, while none of the CTRL cells were arrested in G1, n = 165 for CTRL and n = 160 for FADD KD from three independent experiments. Error bars represents mean ± SEM. *$p < 0.05$; **$p < 0.01$; ***$p < 0.001$ and ****$p < 0.0001$. *G*, quantification of number of cells that underwent at least one mitotic event during the 48 h live cells imaging experiment revealed that 100% of CTRL cells underwent mitosis, in contrast to only 5% of FADD KD cells. Error bars show the mean of three independent experiments ± SEM. Each *dot* represents average number of mitotic events per experiment with at least 100 cells analyzed per experiments. *$p < 0.05$; **$p < 0.01$; ***$p < 0.001$ and ****$p < 0.0001$. *H*, Western blot analysis of CTRL (*left panel*) and FADD KD (*right panel*) cells synchronized in G2/M using the CDK1 inhibitor, CDK1i, and samples were collected at indicated timepoints after release from the block. Immunoblots were probed using S-phase and G2/M phase markers cyclin B1, cyclin A2, Securin, pRB, Phospho Histone-3, Aurora A, p27 as well as FADD and α-actinin as controls. CTRL cells show mitotic exit at approximately 8 h (degradation of cyclin A2, cyclin B1, Aurora A and Securin) and a transition from G1 to S was observed at 24 h post G2/M release (as observed by accumulation of cyclin A2, cyclin B1 and Securin). In contrast, FADD KD cells fail to accumulate each of these S phase markers at the expected time. *I*, quantification of cyclin B1 and cyclin A2 levels in CTRL and FADD knockdown NCI-H441 cells synchronized at G2/M using the CDK1 inhibitor, CDK1i. CTRL cells show an accumulation of cyclin B1 (*top panel*) and cyclin A2 (*bottom panel*) upon transition from G1 to S (*green line*), while FADD KD cells (*red line*) demonstrate a decreased efficiency of accumulation of each S phase cyclin. Error bars show mean values from three independent experiments with ± SEM. cyclin B1 and cyclin A2 were normalized to their respective mitotic levels. CTRL, Control; FADD, Fas-associated protein with death domain; NLS, nuclear localization signal.

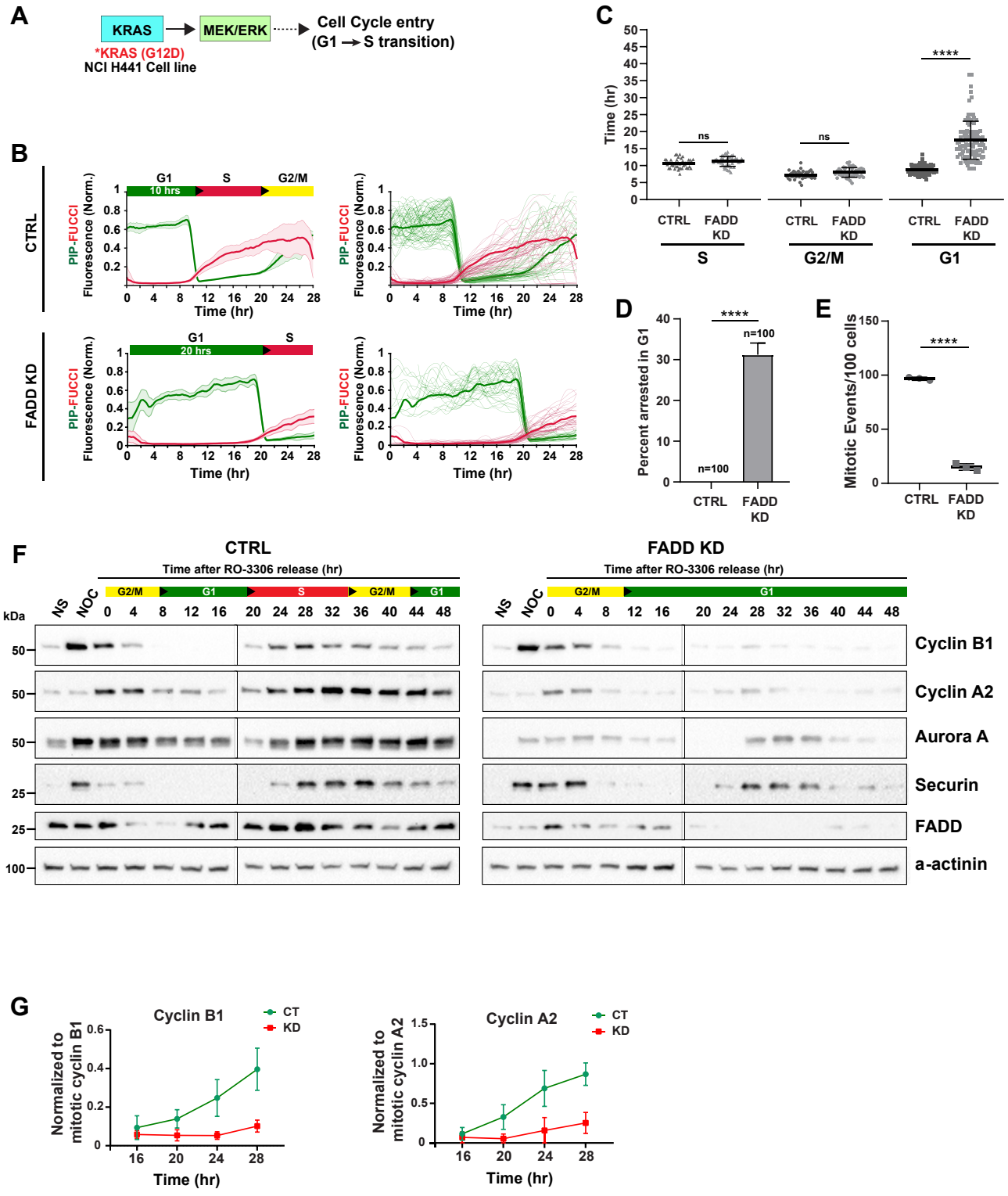

Figure 2. FADD is required for efficient cell cycle entry in KRAS mutant lung cancer cells. *A*, schematic of mutant KRAS-mediated activation of the KRAS-MEK-ERK mitogenic signaling pathway in NCI-H44 cells. *B*, single cell traces of control siRNA (CTRL) or FADD siRNA (FADD KD)–treated NCI-H441 cells stably expressing the PIP-FUCCI reporter. Fluorescence traces were aligned *in silico* at the G1 to S transition (sharp decrease in Cdt1-mVenus signal and a steady increase in Geminin-mCherry signal). The first panel shows the mean of the median traces (*bold plot*) of three independent experiments with variance shown in a *lighter shade*. Individual fluorescence traces of single cells (Cdt1-mVenus and Geminin-mCherry) are also shown. CTRL cells demonstrated a 10 h G1 phase, while FADD KD cells were in G1 for 20 h. n = 85 for CTRL and 65 for FADD KD cells. *C*, quantification of average time spent in S, G2/M, and G1 phase by CTRL and FADD KD NCI-H441 cells reveal that in contrast to 10 h G1, FADD KD cells had a G1 time of >20 h whereas there was no significant difference in previous S and G2/M times in CTRL *versus* FADD KD cells. n = 45, n = 42 and n = 105 for S, G2/M and G1 phases, respectively. Quantifications are from three independent experiments. Error bars represents mean ± SEM. *$p < 0.05$; **$p < 0.01$; ***$p < 0.001$; and ****$p < 0.0001$, n.s. = non-significant. *D*, bar graph showing percentage of cells arrested in G1 in CTRL or FADD KD NCI-H441 cells. 30% of FADD KD cells demonstrated an arrest in G1 compared to 0% of CTRL cells (*left panel*). n = 100 for CTRL and n = 100 for FADD KD. Error bars represents mean ± SEM. *$p < 0.05$; **$p < 0.01$;

and (22). MEFs that harbor mutant KRAS (but wild type for FADD) exhibited rapid proliferation, upon AdCre administration which initiates the expression of oncogenic $KRAS^{G12D}$. In contrast, MEFs that were conditionally deleted for the FADD transgene and expressed $KRAS^{G12D}$ exhibited a lower rate of proliferation (Fig. S4*C*) and (22), indicating that FADD is also required for entry into the cell cycle in non-transformed cells, in context of mutant KRAS as a mitogenic driver.

The significance of APC/C-Cdh1 inactivation during the G1 to S transition has best been studied in HeLa cells (11, 14, 15, 33). To evaluate the contribution of FADD in APC/C-Cdh1 inactivation in this model system we utilized HeLa cells expressing mCherry conjugated to a peptide from Geminin containing its APC/C degron motif (34). APC/C activity heatmaps and individual cell traces show that HeLa cells with FADD knockdown have hyperactive APC/C-Cdh1 and elongated G1 with slower APC/C turn-off rates compared to the control cells (Fig. S5, *A–D*). Since FADD-depleted cells spend more time in G1, their intermitotic times also increase (Fig. S5*E*), further confirming that FADD depletion disrupts the G1 to S transition. To further support a requirement for FADD in APC/C-Cdh1 inactivation in HeLa cells, we conducted a transient CRISPR/Cas9 mediated ablation of the FADD locus using two independent sgRNA. Western blot analysis of FADD-deleted cells showed a modest decrease in the rate of accumulation of mitotic cyclins cyclin B1, Aurora A, and Securin (Fig. S6*A*) upon G1 to S transition in cells released from a G2/M arrest (nocodazole). The dependence on FADD during the G1 to S transition in HeLa cells was less pronounced compared to NCI-H1975, NCI-H441, HCC827, and MCF-7 cells. This difference could be attributed to the fact that HeLa cells express HPV18 proteins E6 and E7, which lead to hyper-phosphorylation of Rb and constitutive activation of the E2F transcription factor. Constitutively active E2F leads to the expression of S-phase cyclins (cyclin E) and Emi1. Emi1 and cyclin-E/CDK2 inactivate APC/C-Cdh1 promoting the entry of cells into S phase. We hypothesize that due to hyperactive E2F, HeLa cells are less responsive to FADD depletion compared to lung adenocarcinoma cell lines (summarized in Fig. S6*B*). We evaluated the relative levels of FADD and Emi1 in HeLa, NCI-H441, and NCI-H1975 and found that indeed, HeLa cells express relatively high Emi1 protein levels compared to NCI-H1975 and NCI-H441 cells, which have reduced Emi1 levels and elevated FADD levels in contrast (Fig. S6*C*), suggesting that FADD may be a major driver of G1 to S transition in lung adenocarcinoma cells, a function that is carried out predominantly by Emi1 rather than FADD in HeLa cells.

FADD depletion leads to hyperactive APC/C-Cdh1

To investigate if an inability to accumulate S phase cyclins could be due to APC/C-Cdh1 hyperactivity, control and FADD knockdown NCI-H441 cells were synchronized at G2/M using CDK1i. At 20 h post CDK1i release (exiting G1 and entering S phase), cells were treated with a proteasomal inhibitor (MG132), APC/C inhibitor (pro-TAME), or an inhibitor of APC/C-Cdc20 (APCin) for 10 h (Fig. 3*A*). CTRL cells demonstrated high levels of cyclin B1 in S phase (Fig. 3*B*, CTRL, dimethyl sulfoxide [DMSO] treated), which did not change in the presence of MG132, pro-TAME, or APCin, indicating that ubiquitination and proteasomal degradation of cyclin B1 was not occurring in control cells at this time point (due to APC/C-Cdh1 inactivity in S phase). In contrast, FADD-depleted cells had barely detectable levels of cyclin B1 under identical conditions (Fig. 3*B*, DMSO in FADD KD), while MG132 as well as pro-TAME but not APCin treatment restored the levels of cyclin B1 when compared to DMSO-treated cells (Fig. 3*B*). Restoration of APC/C-Cdh1 substrate levels upon inhibition of APC/C (Pro-TAME) or the proteasomal machinery (MG132) but not APC/C-Cdc20 (APCin) in FADD-depleted cells supports the notion that the APC/C-Cdh1 E3-ligase (and not APC/C-Cdc20) remains hyperactive in the absence of FADD during the G1 to S transition. Furthermore, to directly demonstrate APC/C-Cdh1 hyperactivity in FADD-depleted cells, APC/C complexes were extracted from G1 synchronized cells. APC/C-Cdh1 was immunopurified from control and FADD siRNA treated cells using CDC27 antibody and evaluated for *in vitro* E3-ligase activity using recombinant cyclin B1 as a substrate. Both samples were analyzed prior to immunoprecipitation of G1 synchronized cells (Fig. S7*A*, input), and after immunoprecipitation using a CDC27 antibody (Fig. S7*A*, CDC27 IP), which revealed similar levels of APC/C components, but differences in FADD levels as well as cyclin B1 levels in FADD knockdown input samples. An *in vitro* cyclin B1 ubiquitination assay of the immunopurified samples demonstrated enhanced ubiquitination activity over time in FADD-depleted cells compared to the control cells (Fig. S7*A*, rightmost panel, quantification shown in Fig. S7*B*). This indicates that APC/C-Cdh1 is hyperactive in the absence of FADD, consistent with our earlier observation (Figs. 1, 2 and 3*B*) that levels of APC/C-

$^{***}p < 0.001$ and $^{****}p < 0.0001$, n.s. = non-significant. *E*, percentage of CTRL and FADD KD NCI-H441 cells that underwent mitosis during 48 h of imaging. Each data point represents a total of at least 100 cells from a single experiment. 100% of CTRL cells underwent mitosis whereas only 10% of FADD KD cells underwent mitosis during the entire imaging period. Error bars shows the mean of three independent experiments ± SEM. n = 300 for CTRL and n = 200 for FADD KD cells from three independent experiments. Error bars represents mean ± SEM. $^{*}p < 0.05$; $^{**}p < 0.01$; $^{***}p < 0.001$; and $^{****}p < 0.0001$. *F*, Western blot analysis of CTRL (*left panel*) and FADD KD (*right panel*) cells synchronized in G2/M using CDK1i, and samples were collected at indicated timepoints after release from the block. Immunoblots were probed using S-phase and G2/M phase markers cyclin B1, cyclinA2, Securin, pRB, Phospho Histone-3, Aurora A, as well as FADD and α-actinin as controls. CTRL cells show mitotic exit at approximately 4 h (degradation of cyclin A2, cyclin B1, Aurora A and Securin) and a transition from G1 to S was observed at 20 h post G2/M release (as observed by accumulation of cyclin A2, cyclin B1 and Securin). In contrast, FADD KD cells fail to accumulate each of these S phase markers at the expected time. *G*, quantification of cyclin B1 and cyclin A2 levels in CTRL and FADD knockdown NCI-H441 cells synchronized at G2/M using CDK1i. Control (CT) cells show an accumulation of cyclin B1 (*left panel*) and cyclin A2 (*right panel*) upon transition from G1 to S (*green line*), while FADD KD cells (*red line*) demonstrate a decreased efficiency of accumulation of each S phase cyclin. Error bars show mean values from three independent experiments with ± SEM. cyclin B1 and cyclin A2 were normalized to their respective mitotic levels. CTRL, Control; FADD, Fas-associated protein with death domain.

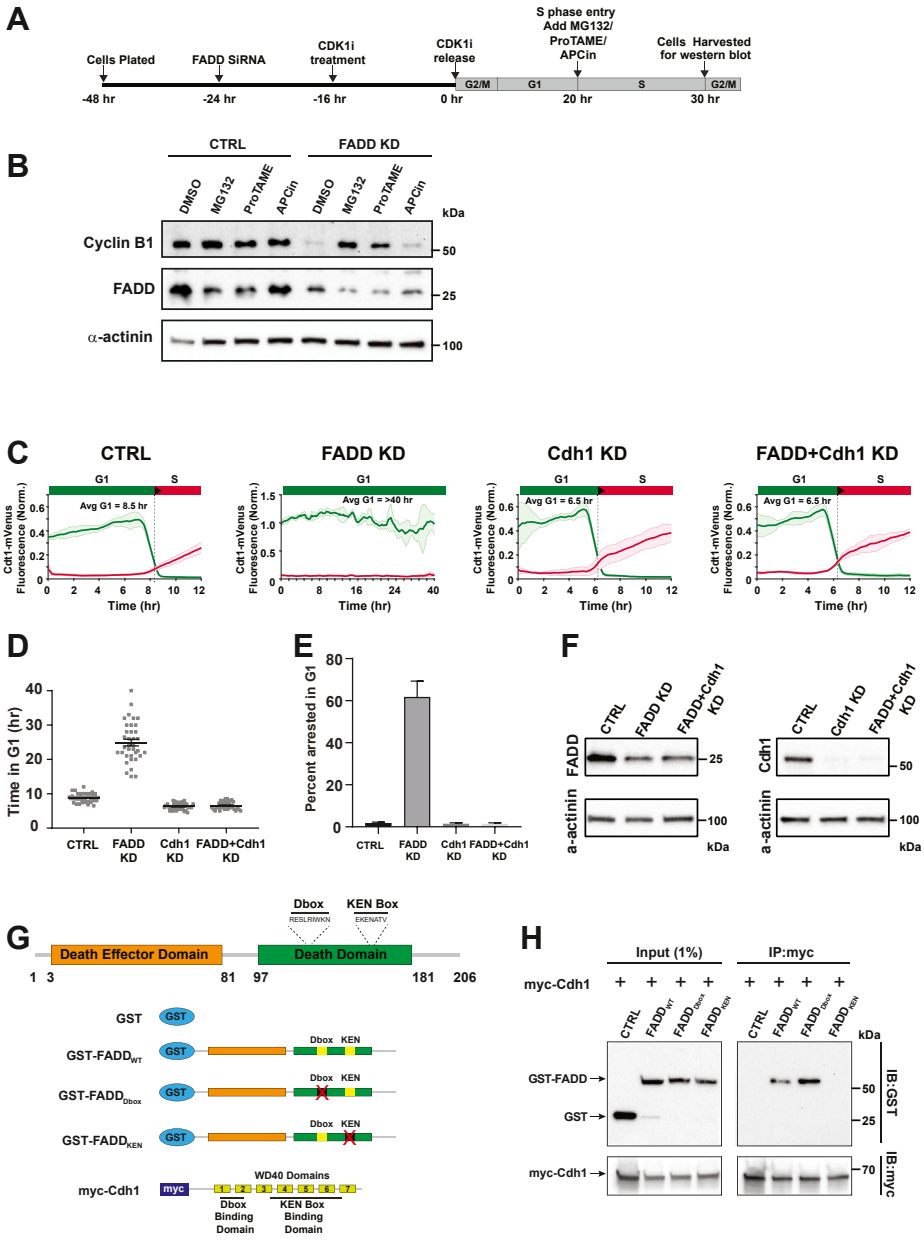

Figure 3. APC/C-Cdh1 ubiquitin ligase hyperactivity in FADD depleted cells requires Cdh1 expression. *A*, a schematic of the experimental design to investigate if failure to accumulate cyclin B1 during the G1 to S transition in the absence of FADD can be ascribed to hyperactive APC/C-Cdh1. Cells arrested at G2/M (using CDK1i) were released into G1 and treated with inhibitors of APC/C or the proteosome at the expected time for G1 to S transition (20 h). Cell extracts were prepared and analyzed for cyclin B1 levels 10 h post-treatment. *B*, immunoblot analysis for cyclin B1 levels in control siRNA-transfected (CTRL) as well as FADD siRNA transfected (FADD KD) cells treated with DMSO, MG132, ProTAME, or APCin. In contrast to DMSO-treated CTRL cells, FADD KD cells has decreased levels of cyclin B1. Treatment with MG132 (proteasomal inhibitor) and ProTAME (APC/C inhibitor) but not APCin (APC/C-Cdc20 inhibitor) resulted in an increase in cyclin B1 levels in FADD KD cells but not CTRL cells (*bottom panel*). *C*, live cell imaging of control siRNA (CTRL), FADD siRNA (FADD KD), Cdh1 siRNA (Cdh1 KD), and FADD+Cdh1 siRNA (FADD+Cdh1 KD) treated cells was used to acquire fluorescence emission traces over a >40 h time period. Graphs shown are the mean of the median traces from the two independent experiments with variance shown in a *lighter shade*. CTRL cells demonstrated a 8.5 h time in G1, while a majority of FADD KD cells were in G1 during the entire imaging period of 48 h. Cdh1 KD cells demonstrated a reduced G1 time of 6.5 h compared to CTRL cells (8.5 h) whereas simultaneous knockdown of FADD and Cdh1 also resulted in reduced G1 times of 6.5 h. *D*, quantification of average time spent in G1 phase by CTRL, FADD KD, Cdh1 KD, and FADD+Cdh1 KD NCI-H1975 cells. CTRL cells exhibited a 8.5 h time in G1 while FADD KD cells had a G1 time of 24 h. Cdh1 KD and FADD+Cdh1 KD cells had reduced mean time in G1 of 6.5 h. n = 50 cells for all conditions from two independent experiments. Error bars represents mean ± SEM. *$p < 0.05$; **$p < 0.01$; ***$p < 0.001$ and ****$p < 0.0001$, n.s. = non-significant. *E*, bar graph showing percentage of cells arrested in G1 in CTRL, FADD KD, Cdh1 KD, and FADD+Cdh1 KD NCI-H1975 cells. 70% of FADD KD cells demonstrated an arrest in G1 compared to <2% in CTRL, Cdh1 KD, and FADD+Cdh1 KD cells. n = 50 from two independent experiments. Error bars represents mean ± SEM. *$p <$ 0.05; **$p < 0.01$; ***$p < 0.001$ and ****$p < 0.0001$, n.s. = non-significant. *F*, Western blot analysis of CTRL, FADD KD, Cdh1 KD and FADD+Cdh1 KD NCI-H1975 cells collected 48 h after siRNA treatment. Immunoblots were probed using Cdh1, FADD or α-actinin antibodies. *G*, functional domains within human FADD showing the Death Effector Domain at the N-terminus and the Death Domain at the C-terminus, as well as putative D-box and KEN-box motifs (*top panel*). Expression constructs used to investigate the interaction of FADD with Cdh1. GST-tagged FADD$_{WT}$, FADD$_{Dbox}$ (RESL to AAAA), and FADD$_{KEN}$ (KEN to AAA) mutants of FADD as well as with myc-tagged human Cdh1 were constructed. *H*, lysates from HEK293FT cells expressing the indicated constructs were immunoprecipitated using myc antibodies (myc-trap nanobodies) to immunoprecipitate myc-Cdh1. The precipitates were immunoblotted with myc antibody to detect the immunoprecipitated myc-CDH1 as well as a GST antibody to detect GST-FADD coimmunoprecipitation. FADD, Fas-associated protein with death domain.

Cdh1 substrates including cyclin B1, cyclin A2, cyclin E, Aurora A, and Securin fail to accumulate in FADD-depleted NCI-H1975, NCI-H441, and HCC827 cells, resulting in a defect in the G1 to S transition. To further confirm that the enhanced E3-ligase activity observed in FADD-depleted cells could be directly attributed to the APC/C-Cdh1, we co-depleted Cdh1 simultaneously with FADD using NCI-H1975 cells. CTRL cells required 8.5 h in G1 prior to a transition into S while a majority of FADD-depleted cells (FADD KD, Fig. 3*C*) demonstrated a G1 arrest during the entire imaging period (quantified in Fig. 3, *D* and *E*). Depletion of Cdh1 alone in NCI-H1975 cells resulted in an accelerated G1 to S transition (Fig. 3*C*), wherein the 8.5 h G1 residence time in CTRL cells was shortened to 6.5 h in Cdh1 KD (quantified in Fig. 3*D*). Most interestingly, cells having a simultaneous depletion of FADD and Cdh1 also required 6.5 h to undergo a G1 to S transition (Fig. 3*C*, quantified in Fig. 3*D*), wherein less than 2% of the cells demonstrated a G1 arrest (Fig. 3*E*) despite the absence of FADD expression (Fig. 3*F*). These findings provide support for the notion that the G1 arrest (as a result of APC/C-Cdh1 hyperactivity) observed in response to FADD depletion requires Cdh1, the substrate binding coactivator subunit of the APC/C-Cdh1 E3-ligase, and that the observed delay in the G1 to S transition in FADD depleted cells is dependent on the presence of Cdh1 and thus APC/C-Cdh1 specific.

A consensus KEN-box domain at the C-terminus of FADD is required for interaction with Cdh1 and inactivation of APC/C-Cdh1

The current understanding is that APC/C-Cdh1 is inactivated upon phosphorylation by CDKs as well as through direct binding and inhibition of its enzymatic activity by Emi1 through a pseudosubstrate mechanism (3, 35). Since FADD, like Emi1, also contains a consensus Cdh1/Cdc20 interacting D-Box motif (RESLR), as well as a KEN-Box (KEN) at the C-terminus (Fig. 3*G*), we hypothesized that it may function similar to Emi1. To test this, we evaluated the ability of FADD to interact with Cdh1 using HEK-293FT cells. Indeed, immunoprecipitation of myc-tagged Cdh1 resulted in co-immunoprecipitation of $FADD_{WT}$ (Fig. 3*H*) in cells co-expressing GST-tagged FADD and myc-tagged Cdh1. An interaction of FADD ($FADD_{WT}$) with Cdh1 was further confirmed by immunoprecipitation of GST-tagged FADD, which resulted in a co-immunoprecipitation of Cdh1 (HA-Cdh1, Fig. S7*C*). Most interestingly, mutation of the KEN-box (to AAA, $FADD_{KEN}$), abrogated the interaction of FADD with Cdh1, while mutation of the D-Box (RESL to AAAA, $FADD_{Dbox}$) did not (Figs. 3*H* and S7*C*), demonstrating that FADD utilizes its KEN-box domain to interact with Cdh1. These studies further revealed that FADD also interacts with Cdc20, the substrate-binding co-activator of the APC/C during mitosis (Fig. S7*D*). However, in contrast to the requirement of the KEN-box for FADD's interaction with Cdh1, our co-immunoprecipitation studies suggest that the interaction of FADD with Cdc20 may require the presence of the D-box (Fig. S7*D*), wherein the $FADD_{Dbox}$ mutant of FADD co-immunoprecipitated with Cdc20 less efficiently compared to $FADD_{WT}$ or $FADD_{KEN}$.

Next, we asked if overexpression of wild-type or mutants of FADD impacted G1 to S transition of the cell cycle (experiment outlined in Fig. 4*A*). We engineered our PIP-FUCCI expressing NCI-H441 cells, for expression of a FADD transgene in a doxycycline-dependent manner. Live cell imaging of conditional $FADD_{WT}$ or $FADD_{Dbox}$ overexpressing cells (Fig. 4*B*) did not show any obvious alteration in the G1 to S transition, wherein APC/C-Cdh1 inactivation as quantified by Geminin-mCherry accumulation occurred at approximately 18 h in each of the conditions, after releasing from CDK1i when compared to empty vector control cells (NT CTRL, Fig. 4*B*). In contrast, $FADD_{KEN}$ overexpression resulted in delayed APC/C-Cdh1 inactivation (>24 h) as well as a significant fraction (38%) of cells failing to enter the S phase throughout the entire imaging period. A defect in APC/C-Cdh1 inactivation in $FADD_{KEN}$ overexpressing cells was validated through the analysis of the level of its substrates after release from a G2/M arrest. Control cells (NT CTRL, Fig. 4*C*), as well as $FADD_{WT}$ or $FADD_{Dbox}$ overexpressing cells, demonstrated similar kinetics for APC/C-Cdh1 inactivation, as evidenced by accumulation of cyclin B1, cyclin A2, and Securin at 20 h post CDK1i release (entry into S) for each cell line (Fig. 4*C*). This was in contrast to $FADD_{KEN}$ expressing cells, wherein cyclin B1, cyclin A2, and Securin levels were observed to be lower immediately upon release (suggesting arrest in G1) and a failure to accumulate each of the APC/C-Cdh1 substrates at the expected time post CDK1i release ($FADD_{KEN}$, Fig. 4*C*). Quantitative analysis of replicate western blots confirmed that the accumulation of cyclin B1 observed at approximately 16 h post-release in control cells (CTRL, Fig. 4*D*) was not observed upon conditional overexpression of the $FADD_{KEN}$ mutant. We also performed quantification of mitotic events per 100 cells over 72 h and found that 100% of control (NT CTRL, Fig. 4*E*), $FADD_{WT}$, and $FADD_{Dbox}$ cells underwent at least one round of mitosis whereas only 30% of $FADD_{KEN}$ cells underwent mitosis further demonstrating that $FADD_{KEN}$ overexpression leads to a delayed G1 to S transition.

A defect in Geminin-mCherry accumulation (Fig. 4*B*) as well as cyclin B1, cyclin A2 and Securin in $FADD_{KEN}$ (Fig. 4*C*), and altered cell cycle kinetics (Fig. 4*E*), suggested to us a dominant negative effect of the $FADD_{KEN}$ mutant such that although unable to bind to Cdh1, it can prevent endogenous wild-type FADD to function as an APC/C-Cdh1 inhibitor, thus allowing APC/C-Cdh1 to be hyperactive when $FADD_{KEN}$ is overexpressed. We directly tested the hypothesis that $FADD_{KEN}$ may be bound to the APC/C complex by immunoprecipitating the APC/C-Cdh1 complex from cells wherein expression of $FADD_{KEN}$ can be conditionally activated using doxycycline. Since $FADD_{WT}$ interacts with Cdh1, it was not unexpected that it would co-immunoprecipitate with APC/C from cells in G1 (Fig. 4*F*). Surprisingly, $FADD_{KEN}$, a mutant that failed to co-immunoprecipitate with Cdh1 (Fig. 3*H*), remained bound to the APC/C and was also able to co-immunoprecipitate with the APC/C (Fig. 4*F*). To further support this finding, we performed a similar experiment, except that Halo-tagged $FADD_{WT}$ was

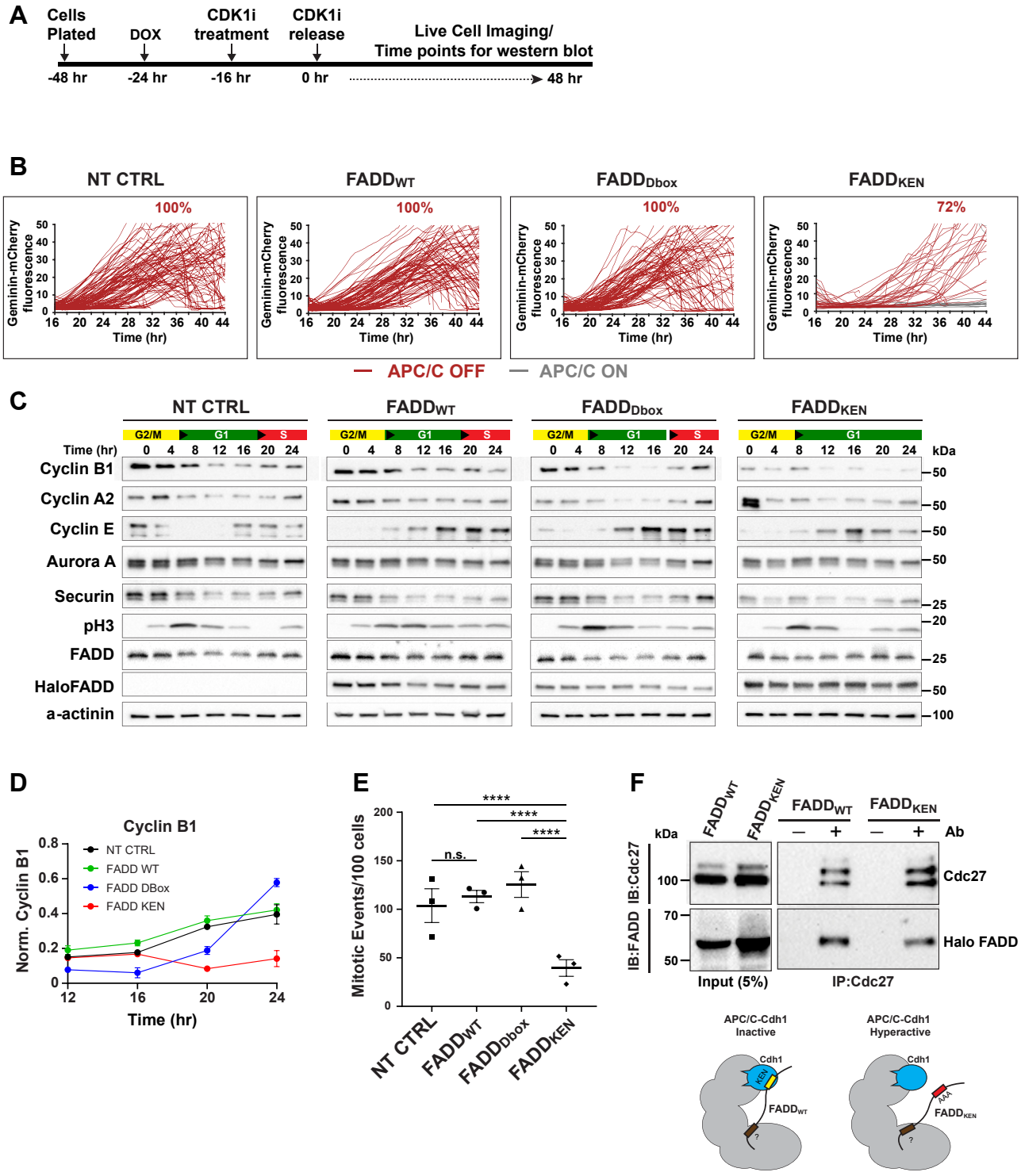

Figure 4. $FADD_{KEN}$ but not $FADD_{WT}$ or $FADD_{Dbox}$ conditional overexpression leads to APC/C-Cdh1 hyperactivity during the G1/S transition. *A*, a schematic of the experimental approach. Doxycycline inducible halo FADD overexpressing NCI-H441 cells were synchronized at G2/M using CDK1i and released. Live cell imaging of cyclin accumulation using Western blot analysis (see below). *B*, single cell traces of NT CTRL, $FADD_{WT}$, $FADD_{Dbox}$, and $FADD_{KEN}$ overexpressing NCI-H441 cells stably expressing PIP-FUCCI reporter synchronized at G2/M using CDK1 inhibitor CDK1i. APC/C-Cdh1 activity was monitored using Geminin-mCherry fluorescence. Accumulation of mCherry fluorescence beginning 16 to 18 h post-release is indicative of APC/C-Cdh1 inactivation during the G1 to S phase transition in no-treatment control cells (NT CTRL). Analogous to NT CTRL cells, 100% of $FADD_{WT}$ and $FADD_{Dbox}$ cells demonstrated accumulation of Geminin-mCherry fluorescence (indicative of APC/C-Cdh1 inactivation) at the expected 16 to 18 h post G2/M release, whereas APC/C-Cdh1 inactivation was delayed (24–32 h) and observed in only 72% of $FADD_{KEN}$ cells. 38% of $FADD_{KEN}$ cells failed to inactivate APC/C-Cdh1 (shown in *grey*) during the 48 h imaging time. n = 100 independent traces of each condition are shown, from at least three independent experiments. *C*, Western blot analysis of NT CTRL as well as inducible $FADD_{WT}$, $FADD_{Dbox}$, and $FADD_{KEN}$ overexpressing NCI-H441 cells were synchronized at G2/M using CDK1i, released and samples were collected at various timepoints for analysis of S-phase and G2/M phase markers cyclin B1, cyclin A2, Securin, Phospho Histone-3, Aurora A, Halo (FADD transgenes are Halo-tagged) and α-actinin. NT CTRL, $FADD_{WT}$ and $FADD_{Dbox}$ cells demonstrate elevated levels of G2/M proteins (cyclin B1, cyclin A2, Aurora A, Securin at 0 h) which are depleted upon mitotic exit (8 h), and reaccumulated upon entry into S as a result of APC/C-Cdh1 inactivation at 20 h post G2/M release. In contrast to NT CTRL as well as $FADD_{WT}$, $FADD_{Dbox}$ overexpressing cells, $FADD_{KEN}$ overexpressing cells demonstrate decreased levels of each of

immunoprecipitated to demonstrate that FADD was bound to the APC/C-Cdh1 complex (Fig. S7*E*). In addition, $FADD_{KEN}$ was demonstrated to co-immunoprecipitate with the APC/C despite its inability to interact with Cdh1 (Fig. S7*E*). Taken together, these findings suggest that like Emi1, FADD may interact with additional components of the APC/C-Cdh1 complex, which provides a possible explanation for the observed dominant-negative phenotype when $FADD_{KEN}$ is overexpressed (depicted in Fig. 4*F*, lower panel).

$FADD_{WT}$ overexpression but not $FADD_{KEN}$ forces APC/C-Cdh1 inactivation in the absence of CDK4/6 activity

The current understanding of the G1 to S transition is that Emi1 and cyclin E/Cdk2 are required for the inactivation of APC/C-Cdh1. Emi1, through its pseudosubstrate inhibitor function and cyclin E/Cdk2 by Cdh1-phosphorylation (Fig. 5*A*). Our findings above suggest that FADD may also function as an inhibitor of APC/C-Cdh1 by binding to Cdh1 through its KEN-box domain. To evaluate the ability of FADD to inactivate APC/C-Cdh1 independent of Emi1 and cyclin E/Cdk2, we treated NCI-H441 cells with a selective cyclin D/CDK4/6 kinase inhibitor (CDK4/6i, Palbociclib). In the absence of CDK4/6 kinase activity, phosphorylation of Rb is inhibited, resulting in a G1 arrest due to sustained E2F inhibition by Rb (Fig. 5*A*). Indeed, cells synchronized in G2/M (using CDK1i) followed by CDK4/6i treatment (experimental design detailed in Fig. 5*B*) demonstrated a diminished capacity for Geminin-mCherry accumulation, wherein only 9% of the cells demonstrated mCherry fluorescence (red plots) at >32 h post CDK1i release (CDK4/6i, Fig. 5*C*), in contrast to 100% at 18 h in untreated cells (NT, Fig. 5*C*). In line with our previous observation (Fig. 2, *B–D*), siRNA-mediated knockdown of FADD in CDK1i-treated cells resulted in 71% of cells showing an extended G1, demonstrated by the accumulation of Geminin-mCherry at >24 h (FADD KD, Fig. 5*C*), while 29% of cells demonstrated a failure to inactivate APC/C-Cdh1 during the entire imaging period (grey plots). Interestingly, FADD depletion using siRNA in combination with CDK4/6i treatment completely abolished the ability of NCI-H441 cells to inactivate APC/C-Cdh1 as evidenced by Geminin-mCherry accumulation in only 1% of cells (CDK4/6i+FADD KD, Fig. 5*C*). Overexpression of $FADD_{WT}$ in CDK4/6i-treated cells resulted in 32% of cells demonstrating Geminin-mCherry accumulation (indicative of APC/C-Cdh1 inactivation) at >24 h (CDK4/6i+$FADD_{WT}$, Fig. 5*D*). Similar to $FADD_{WT}$, overexpression of $FADD_{Dbox}$ also promoted APC/C-Cdh1 inactivation (28%) under conditions when CDK4/6 activity was inhibited by CDK4/6i (CDK4/6i+$FADD_{Dbox}$, Fig. 5*D*). However, $FADD_{KEN}$ overexpression in the presence of CDK4/6i failed to promote APC/C-Cdh1 inactivation as determined by a failure to accumulate Geminin-mCherry fluorescence (CDK4/6i+$FADD_{KEN}$, Fig. 5*D*). The observation that $FADD_{KEN}$ consistently appeared to act as a dominant negative such that in contrast to 8% of control cells (no FADD overexpression) exhibiting Geminin-mCherry accumulation, $FADD_{KEN}$ expressing cells did not show any Geminin-mCherry accumulation during the imaging period, indicating sustained APC/C-Cdh1 hyperactivity, consistent with a dominant negative phenotype observed above (Figs. 4*B* and 5*D*). Population-level biochemical analysis of cells released from a G2/M arrest (CDK1i treatment) into CDK4/6i, supported the finding that $FADD_{WT}$ and $FADD_{Dbox}$ overexpression promoted APC/C-Cdh1 inactivation as demonstrated by the accumulation of cyclin B1, cyclin A2, Aurora A, and Securin 36 h post CDK1i release ($FADD_{WT}$ and $FADD_{Dbox}$, Fig. 5*E*) while in the absence of FADD overexpression, these S phase proteins fail to accumulate in control cells (CTRL, CDK4/6i treatment but absence of FADD overexpression) (Fig. 5*E*, quantitative analysis of replicates shown in Fig. 5*F*). Each of these APC/C-Cdh1 substrates failed to accumulate in the presence of $FADD_{KEN}$ overexpression ($FADD_{KEN}$, Fig. 5, *E* and *F*). This population-level analysis confirmed the single-cell analysis results (Fig. 5*D*) demonstrating that overexpression of $FADD_{WT}$ results in the inactivation of APC/C-Cdh1 (despite the absence of CDK4/6 activity) and promotes the G1 to S transition. These studies also confirmed a dominant negative effect of $FADD_{KEN}$, since APC/C-Cdh1 substrates were at lower levels in $FADD_{KEN}$ overexpressing cells compared to the control cells (Fig. 5, *E* and *F*).

FADD overexpression inactivates APC/C-Cdh1 in the absence of Rb phosphorylation

To investigate if FADD-mediated inactivation of APC/C-Cdh1 precedes Rb phosphorylation, we utilized stable NCI-H441 cells expressing doxycycline-inducible $FADD_{WT}$, $FADD_{Dbox}$, and $FADD_{KEN}$. Rb-phosphorylation status was evaluated using single-cell immunocytochemistry of cells that were in late G1 (such that the ratio of mVenus to mCherry was >4, Fig. 6*A*). In contrast to untreated cells (NT, Fig. 6, *A* and

these proteins in G2/M (0 h) as well as a failure to efficiently accumulate cyclin A2, cyclin B1, and Securin at the expected time. *D*, quantification of cyclin B1 in NT CTRL, $FADD_{WT}$,$FADD_{Dbox}$ and $FADD_{KEN}$ NCI-H441 cells synchronized at G2/M using CDK1i. Control (NT CTRL), $FADD_{WT}$, and $FADD_{Dbox}$ cells show an accumulation of cyclin B1 upon transition from G1 to S while $FADD_{KEN}$ cells demonstrate a decreased efficiency of accumulation of cyclin B1. Error bars show mean values from two independent experiments with ± SEM. cyclin B1 was normalized to its 0 h timepoint level. *E*, percentage of NT CTRL, or doxycycline-inducible $FADD_{WT}$, $FADD_{Dbox}$, and $FADD_{KEN}$ overexpressing NCI-H441 cells undergoing mitosis during 48 h of imaging (Imaging was initiated 24 h after the knockdown). Each data point represents a total of at least 100 cells from a single experiment. Error bars show the mean of three independent experiments ± SEM. *$p < 0.05$; **$p < 0.01$; ***$p < 0.001$; and ****$p < 0.0001$, n.s., non-significant. *F*, lysates from G1 synchronized (as described in Fig. 5*A*) NCI-H441 cells expressing indicated doxycycline-inducible Halo-tagged $FADD_{WT}$ or Halo-tagged $FADD_{KEN}$ (KEN to AAA) were immunoprecipitated using Cdc27(APC3) specific antibodies to immunoprecipitate the entire APC/C complex. Lysates were immunoblotted using Cdc27 or FADD antibodies. 10% immunocomplexes were immunoblotted with Cdc27 antibodies whereas 90% immunocomplexes were immunoblotted with FADD antibodies to detect co-immunoprecipitated $FADD_{WT}$ or $FADD_{KEN}$ along with Cdc27 (*upper panel*). Reverse IP of the same samples to confirm APC/C-Cdh1 interaction are shown in Fig. S7*E*. The adjacent cartoon presents our working model for FADD dependent inactivation of APC/C-Cdh1 through its KEN-box dependent interaction with Cdh1. $FADD_{WT}$ inhibits APC/C-Cdh1 during the G1 to S transition. Based on the above results, we propose that $FADD_{KEN}$ interaction with a different subunit of the APC/C but not Cdh1 leads to APC/C-Cdh1 hyperactivity in a dominant-negative fashion, wherein endogenous wild-type FADD is unable to inhibit APC/C-Cdh1 activity. FADD, Fas-associated protein with death domain.

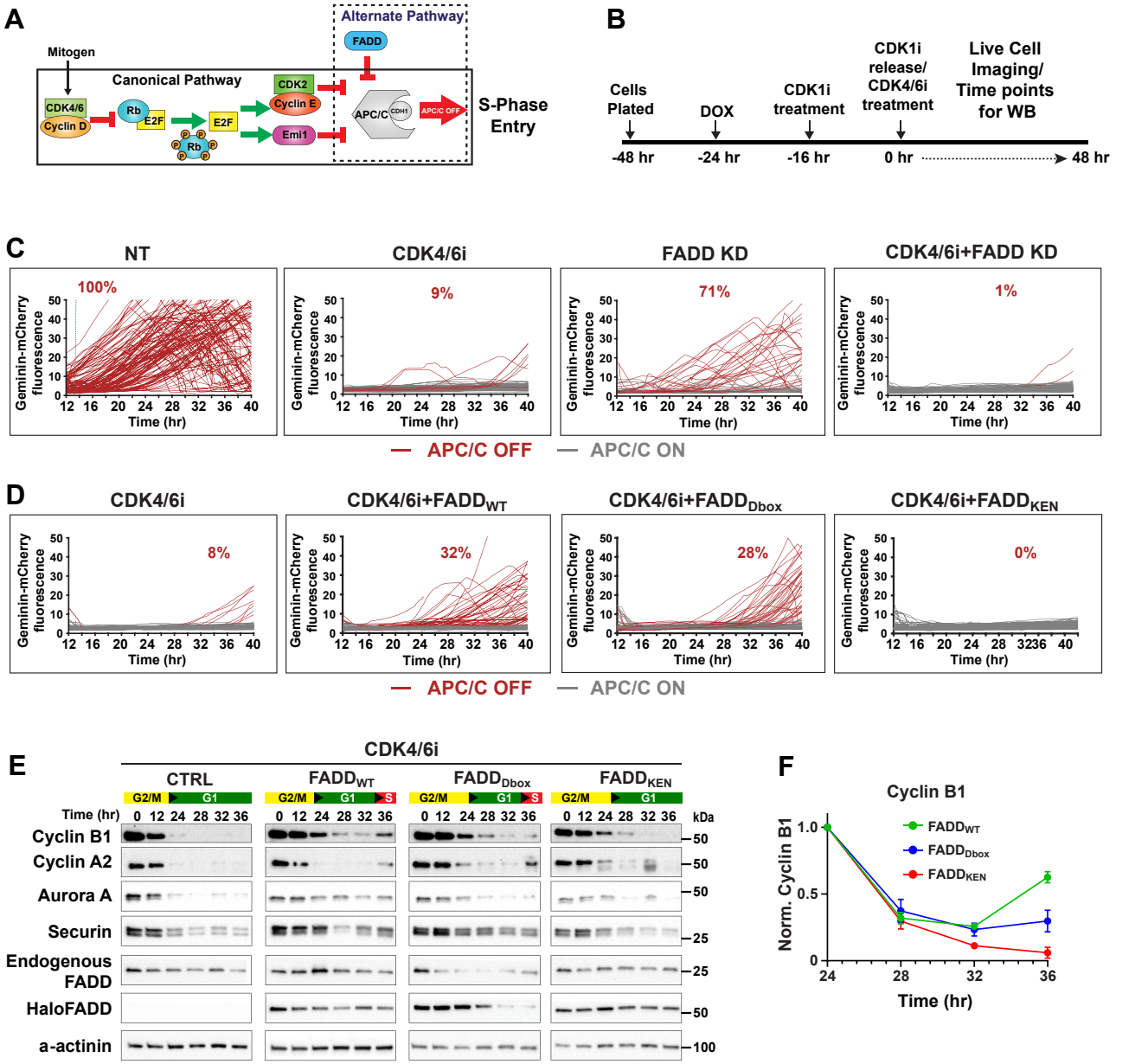

Figure 5. FADD overexpression inactivates APC/C-Cdh1 independent of CDK4/6 activity. *A*, a schematic of mechanisms driving mitogen mediated APC/C-Cdh1 inactivation and cell cycle entry. Mitogenic signals lead to Rb-phosphorylation and release of E2F from inhibition, allowing for transcription of cyclin E and Emi1. Cyclin E/Cdk2-mediated Cdh1 phosphorylation as well as direct inhibition of the APC/C-Cdh1 by Emi1 as a pseudosubstrate is required for transition from G1 to S and cell cycle entry. Our novel finding that like Emi1, FADD also binds and inactivates APC/C-Cdh1 which is required for efficient transition from G1 to S. *B*, a schematic of the experimental approach to investigate the contribution of FADD in APC/C-Cdh1 inactivation in the absence of CDK4/6 activity. Conditional expression of $FADD_{WT}$, $FADD_{Dbox}$, and $FADD_{KEN}$ transgenes in NCI-H441 cells, after synchronization at G2/M using CDK1i was followed by release in the presence of CDK4/6i (palbociclib). Live cell imaging over 48 h as well as Western blots analysis of parallel cultures was conducted at specific time intervals. *C*, single cell traces of NT CTRL, $FADD_{WT}$, $FADD_{Dbox}$, and $FADD_{KEN}$ NCI-H441 cells stably expressing Geminin-mCherry were synchronized at G2/M using CDK1i. mCherry fluorescence of single cells were quantified and show accumulation of Geminin-mCherry beginning 16 h post-release, indicative of APC/C-Cdh1 inactivation in NT CTRL cells. In contrast, only 71% of FADD siRNA-treated cells (FADD KD) demonstrated APC/C-Cdh1 inactivation which was delayed (20–32 h *versus* 16 h in CTRL). In all, 29% of FADD KD cells failed to show mCherry accumulation during the entire experiment (*grey traces*) indicating a failure to inactivate APC/C-Cdh1 and arrest in G1. Inhibition of CDK4/6 activity by treatment with CDK4/6i resulted in 91% of cells failing to demonstrate Geminin-mCherry accumulation. When FADD knockdown and CDK4/6i treatment are combined (CDK4/6i + FADD KD), only 1% of cell population demonstrate accumulation of red fluorescence. n = 100 independent traces of each condition are shown, from at least three independent experiments. *D*, single cell traces of Geminin-mCherry accumulation (a surrogate for APC/C-Cdh1 inactivation) in CDK4/6 inhibited cells (CDK4/6i), in the presence or absence of FADD overexpression ($FADD_{WT}$, $FADD_{Dbox}$, and $FADD_{KEN}$) using NCI-H441 cells. In CDK4/6-inhibited cells, 8% of cells demonstrate Geminin-mCherry accumulation, which was delayed (>32 h) post CDK1i release. Overexpression of $FADD_{WT}$ or $FADD_{Dbox}$ in the presence of CDK4/6 inhibition promoted APC/C-Cdh1 inactivation as observed by 32% or 28% cells, respectively, showing Geminin-mCherry accumulation. In contrast, $FADD_{KEN}$ overexpression in the presence of CDK4/6 inhibition resulted in a complete failure to inactivate APC/C-Cdh1 as observed by 0% of cells showing Geminin-mCherry accumulation. The results represent at least 100 cells under each condition and representative of three independent experiments. *E*, immunoblot analysis of CDK4/6i treated cells (CTRL) in the presence of conditional expression of $FADD_{WT}$, $FADD_{Dbox}$ or $FADD_{KEN}$. Cells were synchronized using CDK1i and samples were collected at various timepoints after release. After CDK1i release cells were treated with CDK4/6i. Cells treated with CDK4/6i show peak cyclin B1, cyclin A2, Aurora A, and Securin levels at 0 h (G2/M) which are degraded past 12 h upon mitotic exit. A failure to accumulate S phase proteins beyond 36 h post-release is indicative of APC/C-Cdh1 hyperactivity and a G1 arrest in the absence of CDK4/6 activity. In contrast, overexpression of $FADD_{WT}$ or $FADD_{Dbox}$ promoted APC/C-Cdh1 inactivation as evidenced by accumulation of S phase proteins at 36 h post-release. In contrast, $FADD_{KEN}$

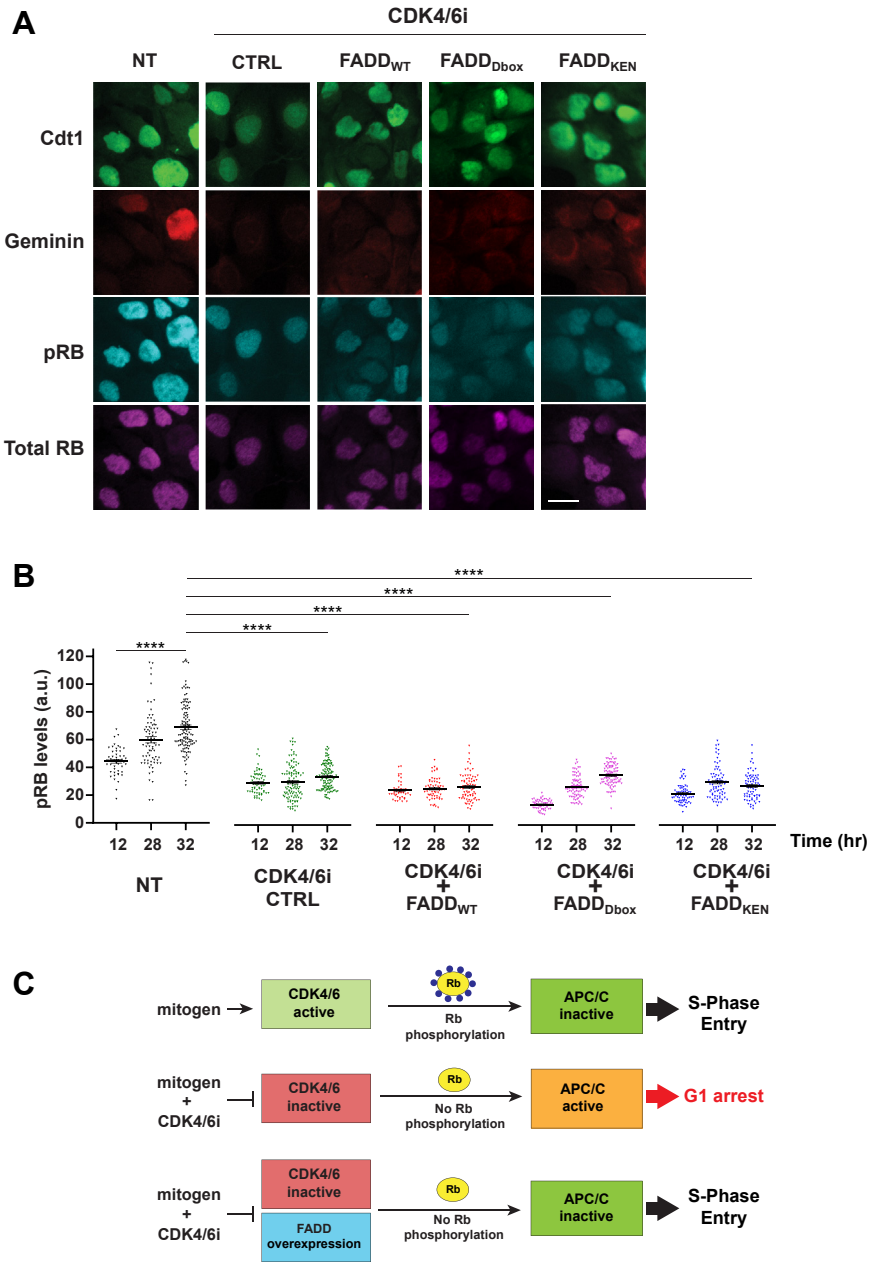

Figure 6. FADD inactivates APC/C-Cdh1 independent of Rb phosphorylation. *A*, representative immunofluorescence images of no-treatment control (NT), CDK4/6i treated control (CTRL), as well as in the presence of $FADD_{WT}$, $FADD_{Dbox}$, and $FADD_{KEN}$ overexpression at 28 h (late G1). NCI-H441 cells synchronized at G2/M using CDK1i and stained using pRB 807/811 or total Rb antibody. NT CTRL cells show robust pRB staining wherein a majority of cells showed high levels of Cdt1-mVenus (Cdt1) fluorescence and an occasional cell having Geminin-mCherry fluorescence indicative of APC/C-Cdh1 inactivation and S-phase transition. In contrast, while cells treated with CDK4/6i have minimal pRB staining. Scale bar is 30 μm. *B*, quantifications of pRB levels in cells shown in panel E above at 12, 28, and 32 h post CDK1i release. Cells expressing three times or more Cdt1-mVenus than Geminin-mCherry were selected for each timepoint. At least 100 cells from three different experiments were used for the quantification. Error bars indicate ± SEM. *$p < 0.05$; **$p < 0.01$; ***$p < 0.001$ and ****$p < 0.0001$, n.s., non-significant. *C*, schematic summarizing findings from Figures 5, and 6, *A* and *B*. In the presence of CDK4/6 activity, Rb phosphorylation leads to APC/C inactivation by Emi1 and cyclin E/CDK2 (*top*). Inhibition of CDK4/6 activity leads to loss of Rb phosphorylation and a failure to inactivate APC/C-Cdh1 leading to a G1 arrest (*middle*). However, exogenous FADD overexpression promotes APC/C-Cdh1 inactivation despite the absence of Rb phosphorylation (*bottom*). FADD, Fas-associated protein with death domain; Rb, retinoblastoma protein.

B), which exhibited robust Rb-phosphorylation at each of the sampling times (12–32 h), CDK4/6i-treated cells, as expected, exhibited low Rb-phosphorylation at each of the time points analyzed post CDK1i release (CTRL, Fig. 6, *A* and *B*). Hence, the observed inactivation of APC/C-Cdh1 in $FADD_{WT}$ and $FADD_{Dbox}$ overexpressing cells (Fig. 5, *D* and *E*) could not be

overexpressing cells demonstrate depleted levels of cyclin B and Aurora A in G2/M (0 h after release) as well as a failure to accumulate S phase proteins up to 36 h post-release from G2/M. *F*, quantification of cyclin B1 in CDK4/6i treated NCI-H441 cells in the presence of conditional expression of $FADD_{WT}$, $FADD_{Dbox}$, or $FADD_{KEN}$. $FADD_{WT}$ and $FADD_{Dbox}$ cells show an accumulation of cyclin B1 upon transition from G1 to S while $FADD_{KEN}$ cells demonstrate a decreased efficiency of accumulation of cyclin B1. Error bars show mean values from two independent experiments with ± SEM. Cyclin B1 was normalized to 1 at its 24 h timepoint level. FADD, Fas-associated protein with death domain.

directly attributed to Rb-E2F reactivation. When CDK4/6 are active, phosphorylation of Rb releases E2F to transcribe Emi1 and cyclin E, which in conjunction with CDK2 activity leads to inactivation of APC/C-Cdh1, enabling transition into S phase. When CDK4/6 activity is inhibited by CDK4/6i, failure to phosphorylate Rb maintains APC/C-Cdh1 in an active state due to the absence of Emi1 and Cyclin E, leading to a G1 arrest. Interestingly, under identical conditions, exogenously overexpressed FADD leads to APC/C-Cdh1 inactivation despite the absence of Emi1 and cyclin E (lack of Rb phosphorylation) (illustrated in Fig. 6*C*). Overall, these results demonstrate that FADD functions as an APC/C-Cdh1 inhibitor independent of Rb phosphorylation (and therefore Emi1 and cyclin E/CDK2). Since CDK2 activity plays an important role in G1 to S transition, we investigated CDK2 activity in FADD siRNA-treated cells using a CDK2 reporter (3, 36). This analysis revealed that in FADD-depleted cells, CDK2 activation was also delayed, in line with the observation that APC/C-Cdh1 remains hyperactive leading to decreased cyclin E levels under these conditions (Fig. S8, *A*–*C*) and hence the delay in G1 to S transition.

Non-apoptotic function of FADD in the cell cycle requires its phosphorylation at Ser-194

Our previous work (21–23) and of others (19, 20, 37, 38) indicate that phosphorylation of FADD at Serine-194, and its nuclear translocation is important in compartmentalizing the distinct functions of FADD in cell division and apoptosis. To investigate the role of Ser-194 phosphorylated FADD in regulating the APC/C-Cdh1 during the G1 to S transition, we conducted rescue experiments, wherein endogenous FADD was depleted using a 3′-UTR targeted siRNA (capable of endogenous FADD KD only) followed by expression of a conditional transgene of Halo-tagged version of $FADD_{WT}$, $FADD_{S194A}$ (non-phosphorylatable mutant) or $FADD_{S194D}$ (phosphomimic). As expected, the depletion of FADD in NCI-H441 cells resulted in a loss of proliferative capacity over 48 h (CTRL compared to FADD KD, Fig. 7*A*). In cells where expression of the Halo-$FADD_{WT}$ was induced simultaneous with endogenous FADD depletion (FADD KD+$FADD_{WT}$, Fig. 7*A*), the loss of proliferative capacity was restored to a large extent. In contrast, in identical experiments wherein $FADD_{S194A}$ or $FADD_{S194D}$ were used to rescue the FADD-depleted cells, proliferative capacity was not restored. Evaluation of the G1 residence time using the PIP-FUCCI reporter demonstrated that in contrast to control cells (CTRL, Fig. 7*B*), FADD-depleted cells (Fig. 7*C*) demonstrated an extended time in G1 (22 h *versus* 10 h in CTRL). However, expression of $FADD_{WT}$ in FADD KD cells resulted in a shortening of the time in G1 (from 22 h in FADD KD to 12 h in FADD KD+$FADD_{WT}$), while neither Ser194 mutants of FADD were able to rescue the protracted G1 in FADD depleted cells. Fig. 7*D* provides a fluorescence image of the same region of interest under each of these conditions over a 24 h period. CTRL cells demonstrated a doubling of cell density at 24 h, and the distribution of cells in G1 (green), S (red) and G2/M (yellow) was unaltered during this period. However, in FADD-depleted cells (FADD KD, Fig. 7*D*), the density of cells remained essentially unchanged between 0 h and 24 h, and a larger fraction of cells were arrested in G1 (green) at either imaging time. In contrast, in cells wherein $FADD_{WT}$ was used to rescue the FADD KD phenotype, a doubling in cell density was observed over the 24 h period, and most significantly, the distribution of cells in G1, S, and G2/M was similar to control cells. Neither the S194 A nor the S194D mutant of FADD was able to rescue the phenotype of FADD-depleted cells (loss of proliferative capacity with an accumulation in G1 (green)). We also performed studies to identify the cellular localization of the FADD in each of these experiments using a fluorescent halo ligand (Janelia 647) that covalently binds to the Halo-tag portion of each of the FADD transgenes (Fig. 7*D*). $FADD_{WT}$ was observed to be localized in the cytosol (predominantly) as well as the nucleus, while the $FADD_{S194A}$ mutant was excluded from the nucleus and the $FADD_{S194D}$ was predominantly located within the nucleus (Fig. 7*E*). This is in agreement with previous studies (20, 21) demonstrating that Ser194 phosphorylation leads to nuclear translocation of FADD. Next, we asked if FADD-phosphorylation was cell cycle-dependent. NCI-H1975 and NCI-H441 cells expressing PIP-FUCCI were stained using a Ser194-phosphorylation-specific FADD antibody. Results in Fig. S9, *A* and *B* demonstrate that the phosphorylated form of FADD is predominantly observed in S and G2/M cells (red and yellow PIP-FUCCI signals respectively), while levels of phosphorylated-FADD were much lower in G1 cells (green) in both NCI-H1975 and NCI-H441 cells. As expected, FADD depletion in either cell line resulted in a G1 arrest (predominantly green cells, FADD KD, Fig. S9, *A* and *B*), and the levels of phosphorylated FADD were significantly diminished. Steady state levels of phosphorylated FADD in either cell line as well as HeLa cells were similar, although levels of total FADD were much lower in HeLa cells and highest in NCI-H1975 cells (Fig. S9*C*).

Discussion

APC/C-Cdh1 activation contributes to mitotic exit, and its activity is required for the maintenance of cells in G1 through proteasomal degradation of key S Phase cyclins and kinases. APC/C-Cdh1 maintains the G1 state, and its inactivation (Restriction Point) is a requisite for cells to commit to entering the cell cycle. Since this commitment is irreversible, the G1 to S transition needs to be robust and tightly regulated and is often dysregulated in cancer (8, 9). Currently, two mechanisms are thought to mediate APC/C-Cdh1 inactivation prior to S-phase entry. Emi1, which is transcriptionally activated by E2F, binds to APC/C-Cdh1 and inhibits its activity as a pseudo-substrate and as a competitive binder with the E2 enzyme Ube2S (12). Additionally, the disassociation of Cdh1 from APC/C upon cyclin E/A-Cdk2 mediated phosphorylation of Cdh1 also inactivates APC/C-Cdh1 enabling entry into S-Phase (3, 4). The studies presented here provide novel

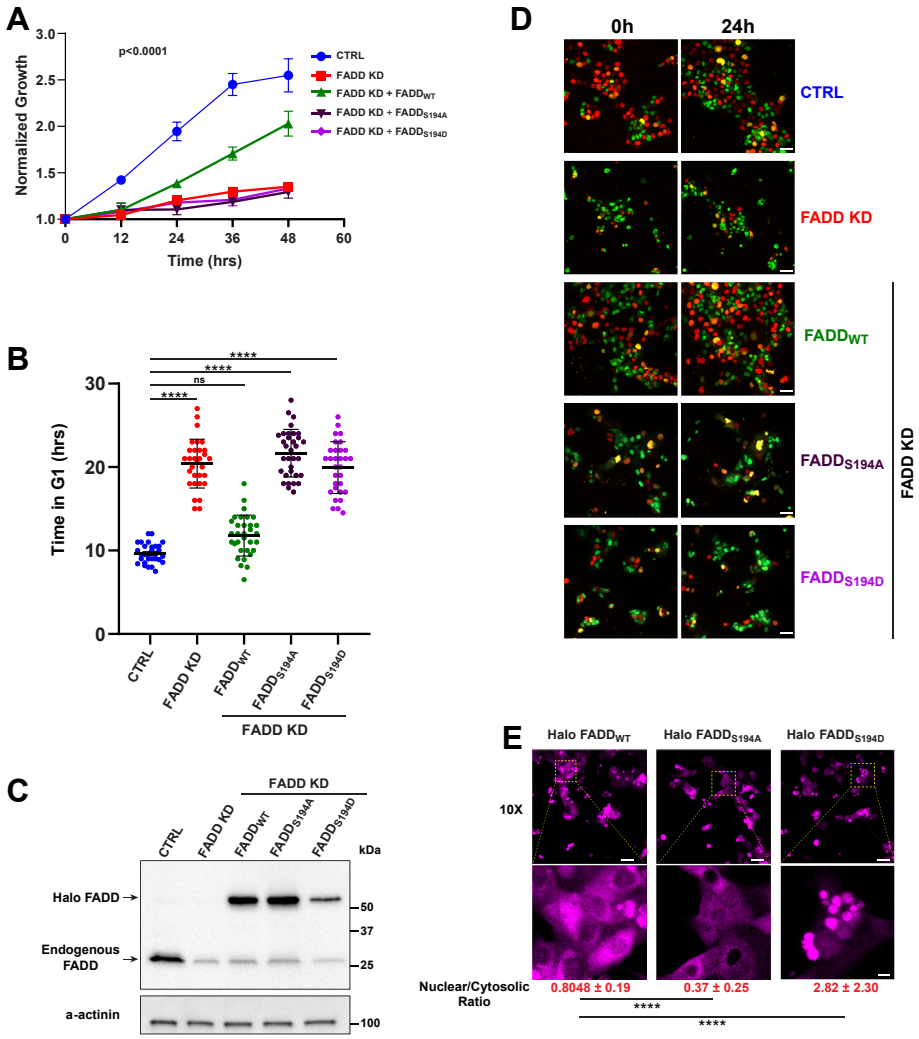

Figure 7. Non-apoptotic function of FADD in the cell cycle requires its phosphorylation at Ser-194. *A*, proliferation of NCI-H441 cells was accessed every 12 h after siRNA transfection. Compared to CTRL cells (*blue*), FADD KD cells (*red*) showed decreased growth rate. FADD siRNA treated cells were rescued using induction of a stable, doxycycline-induced expression of $FADD_{WT}$, $FADD_{S194A}$, and $FADD_{S194D}$ (lack the 3′UTR sequence for siRNA #2). The defect in proliferation of FADD KD was rescued by $FADD_{WT}$ (*green*) but not the $FADD_{S194A}$ (*brown*) or $FADD_{S194D}$ (*pink*) mutants of FADD. Error bars represents mean ± SEM of three independent experiments. Statistical analysis was performed using Two-Way ANOVA for mixed model using Geisser-Greenhouse correction. *B*, quantification of average time spent in G1 phase by CTRL, FADD KD, FADD KD combined with rescue using $FADD_{WT}$, $FADD_{S194A}$, and $FADD_{S194D}$ revealed that in contrast to a 8 to 10 h G1 in CTRL cells, FADD KD cells had a G1 time of >20 h. The extended G1 in FADD KD cells was rescued by exogenously expressed $FADD_{WT}$ but not the $FADD_{S194A}$ or the $FADD_{S194D}$. Single cell computational analysis (n = 30, 31, 32, 33 and 30 for CTRL, FADD KD, FADD KD + $FADD_{WT}$, FADD KD + $FADD_{S194A}$ and FADD KD + $FADD_{S194D}$ respectively) was used to derive the time in G1. Error bars represents mean ± SEM. Statistical significance was measured using a 2-tailed unpaired student *t* test with Welch's correction. ****$p < 0.0001$ and n.s. denotes not significant. *C*, Western blots showing expression of endogenous FADD (CTRL) in NCI-H441 cells transfected with CTRL siRNA or using a 3′ non-coding siRNA(siRNA#2) alone (–). Simultaneous with knockdown of endogenous FADD, expression of a Halo-FADD transgene was initiated using doxycycline to rescue the FADD-depleted phenotype using wild-type FADD (Halo-$FADD_{WT}$), a S194A mutant (Halo-$FADD_{S194A}$), or a S194D mutant (Halo-$FADD_{S194D}$) at 24 h. *D*, fixed immunofluorescence images of CTRL (control siRNA), FADD KD (FADD siRNA#2), FADD KD+$FADD_{WT}$, FADD KD + $FADDS_{194A}$ and FADD KD + $FADD_{S194D}$, of PIP-FUCCI expressing NCI-H441 cells that also carry a conditional Halo-FADD transgene at 0 h and 24 h were collected. Scale bar is 50 μm. *E*, cells from the experiment in (*D*) were stained using Janelia Fluor Halo 646 ligand according to manufacturer's guidelines (see Experimental procedures for details). Images were captured at 10X and zoomed in the inset to show that $FADD_{WT}$ localizes within the nucleus and the cytoplasm whereas $FADD_{S194A}$ is excluded from the nucleus and $FADD_{S194D}$ is mostly restricted to the nucleus. Quantification of Nuclear to Cytosolic fluorescence ratio shown at the *bottom* of the images denote mean fluorescence calculated using atleast 50 cell from three independent experiments ± SEM. Statistical significance was measured using a 2-tailed unpaired student *t* test with Welch's correction. *p* values are reported in the graphs, ****$p < 0.0001$. Scale bar top panel is 50 μm. Scale bar Zoom inset is 10 μm. FADD, Fas-associated protein with death domain.

insights into an additional mechanism that promotes the G1 to S transition, by demonstrating that FADD functions as an APC/C-Cdh1 inhibitor and is required for the G1 to S transition in response to mitogen. The significance of FADD's role in APC/C-Cdh1 inhibition and the G1 to S transition was elaborated by our finding that in the absence of Emi1 and cyclin E-Cdk transcription (as a result of Cdk4/Cdk6 inhibition), overexpression of FADD forced the inactivation of APC/C-Cdh1 despite the absence of Rb phosphorylation. Amplification of the FADD locus at 11q13 and its enhanced expression is observed in head and neck, lung, and breast cancer, which correlates with aggressive disease (21, 39–42), suggesting that dysregulation of the G1 to S checkpoint by FADD may contribute to oncogenesis. FADD is best understood for its function as an adapter for the activation of the extrinsic cell death pathway (17–19). However, findings presented here

wherein FADD is shown to also regulate the cell cycle in response to mitogen are intriguing, in that a single molecule participates in apoptotic cell death and mitogen-mediated cell proliferation. Nuclear translocation of cytosolic FADD upon phosphorylation by CK1α at Serine-194 has been descried by us (21, 22) and others (20, 43), which may represent a molecular event that distinguishes the two disparate activities of FADD. In support, the nuclear Ser-194 phosphorylated form of FADD is associated with cancer and its levels are predictive of clinical outcomes (22, 23, 44). Additionally, results presented here as well as previous studies have shown that expression of a non-phosphorylatable mutant as well as a phosphomimic mutant in cells and mouse models leads to defects in cell proliferation (19, 20, 22, 23, 45) likely due to perturbation of the APC/C activity. Our finding that phosphorylation of FADD is highest in the S and G2/M phase of the cell cycle and lowest in G1, suggests that Ser194-phosphorylation and its nuclear translocation may be required for the transition of cells from G1 to S. The molecular basis for APC/C-Cdh1 inhibition by FADD in analogy to Emi1 and Acm1, two well studied APC/C-Cdh1 inhibitors in mammals and yeast respectively (11, 46), may involve its function as a pseudosubstrate inhibitor of APC/C-Cdh1 mediated by the presence of well-characterized Cdh1 binding motifs, the D-box and the KEN-box at the C-terminus of FADD. Two lines of evidence support this notion. First, the finding that the enhanced E3-ligase activity phenotype (failure to accumulate S-phase cyclins and thus a G1 arrest) observed in FADD-depleted cells required the presence of Cdh1, since cells depleted of Cdh1 and FADD simultaneously failed to demonstrate a G1 arrest. In contrast, a shortened time in G1 was observed as a result of Cdh1 depletion, consistent with previous studies (11, 47). Second, our finding that conditional expression of a heterologous $FADD_{WT}$ transgene could phenotypically rescue cells depleted of endogenous FADD, while conditional expression of the $FADD_{S194A}$ mutant (unable to undergo nuclear translocation) or the $FADD_{KEN}$ mutant (fails to interact with Cdh1) did not restore the G1 arrest observed in FADD depleted cells. This provides compelling evidence that FADD's role in the G1 to S transition requires its nuclear translocation (to colocalize with APC/C-Cdh1) and physical interaction with Cdh1. The finding that the $FADD_{KEN}$ mutant, although unable to interact with Cdh1, remains bound to APC/C-Cdh1 in late G1, and exerts a dominant negative phenotype, suggests that analogous to Emi1, FADD may have additional domains that coordinate its interaction with and inhibition of the APC/C. Future studies will elucidate the structure-function underpinnings of FADD's activity as an APC/C-Cdh1 inhibitor to develop small molecule antagonists of FADD-Cdh1 interaction, which could potentially be used as inhibitor of cell cycle entry in cancer.

Experimental procedures

Cell lines

HEK 293FT cells (Thermo Scientific) were used for all the overexpression and pulldown experiments. NCI-H441 (HTB-174) and HCC827 (CRL-2868) were purchased from ATCC. NCI-H1975 cells were a kind gift from Dr. Dipankar Ray (Radiation Oncology, University of Michigan). HEK 293FT were grown in Dulbecco's modified Eagle's medium (GIBCO), containing 10% fetal bovine serum (FBS) and antibiotics (penicillin-streptomycin). NCI-H441, HCC827 and NCI-H1975 cells were grown in RPMI (Roswell Park Memorial Institute) 1640 Medium (GIBCO) containing 10% FBS and antibiotics (penicillin-streptomycin). All cell lines were grown at 37 °C and 5% CO2. All experiments were conducted with early passage cells that were passaged no more than 15 times. *Mycoplasma* was tested regularly by MycoAlert *Mycoplasma* Detection Kit (Lonza LT07-118).

Antibodies

The following antibodies were used in this study: myc (9E10, SC-131, Mouse monoclonal) 1:1000 WB; cyclin B1 (sc-245, Mouse monoclonal) 1:1000 WB; were from Santa Cruz Biotechnology; FADD (2782, rabbit polyclonal) 1:1000; GST (26H1, mouse monoclonal) 1:1000 WB; cyclin A2 (4656, mouse monoclonal) 1:1000 WB; cyclin E1 (4129, mouse monoclonal) 1:1000 WB; cyclin E1 (13445, rabbit monoclonal) 1:1000 WB; Phospho-Histone H3 (3377, rabbit monoclonal) 1:1000 WB; Aurora A (14475, rabbit monoclonal) 1:1000 WB; α-Actinin (6487, rabbit monoclonal) 1:1000 WB; Rb (9309, mouse monoclonal) 1:100 IF; Phospho-Rb (8516, rabbit monoclonal) 1:1000 WB, 1:350 IF; Phospho-FADD (Ser194) Antibody (Human Specific) (2781 1:1000 WB, 1:100 IF) were from Cell Signaling Technology; Cdh1 (FZR1) (MABT1323 mouse monoclonal) was from Millipore Sigma; Alexa Fluor 405 and Alexa Fluor 647 -conjugated anti-mouse-IgG and anti-rabbit-IgG secondary antibodies (A48258, A32787) were from Thermo Fisher Scientific; (HRP)-conjugated anti-mouse-IgG and anti-rabbit-IgG secondary antibodies were from Jackson Immunoresearch: horseradish peroxidase secondary antibodies (715-035-151, 711-035-152).

Inhibitors

The inhibitors used in this study with their concentrations were as follows: Palbociclib (100 nM, Med Chem Express, HY-50767), CDK1i (10 μM, Sigma-aldrich, SML0569), pro-TAME (15 mM, R&D systems, I44001 M), APCin (30 μM, R&D systems, I44405 M). Nocodazole (0.1 μg/ml, Cell Signaling Technology #2190).

Constructs

The following constructs were used for the interaction studies: myc-Cdh1 was a gift from Pumin Zhang (Addgene plasmid # 28127; http://n2t.net/addgene:28127; RRID:Addgene_28127) (48), pGEX-4T1-$FADD_{WT}$, pGEX-4T1-$FADD_{Dbox}$ and pGEX-4T1-$FADD_{KEN}$ were constructed by PCR cloning human FADD into 5′*EcoRI* and 3′*NotI* restriction sites of the vector pGEX-4T1 (Amersham). pLenti-PGK-Neo-PIP-FUCCI was a gift from Jean Cook (Addgene plasmid # 118616; http://n2t.net/addgene:118616; RRID:Addgene_118616) (28). Tetracycline-inducible ("Tet-On") pTRIPZ lentiviral vectors

(Open Biosystems) were used to PCR clone the N-terminus Halo tagged FADD fusion construct for Halo-tagged $FADD_{WT}$, $FADD_{Dbox}$, $FADD_{KEN}$, $FADD_{S194A}$, and $FADD_{S194D}$ constructs to establish doxycycline-inducible stable cell lines.

siRNA transfection and rescue experiment

NCI-H441, NCI-H1975, and HCC827 cells were transfected using Lipofectamine RNAiMAX reagent (Invitrogen, 13778500) following manufacturer's guidelines. siRNAs were purchased from the Dharmacon SiGenome project: FADD siRNA #1 D-003800-01-0005 (targeting ORF of FADD) and FADD siRNA#2 D-003800-19-0005 (targeting 3′UTR of FADD), control siRNA (non-targeting #1) at a final concentration of 20 nM. Figures 1–3 utilize FADD siRNA#1 whereas Figures. 5 and 7 utilize FADD siRNA#2 (since siRNA targeting 3′UTR does not target the Halo-FADD). Results in each of the key experiments presented were confirmed by both the siRNAs to confirm the accuracy and validity of the knockdown (data not shown). Cdh1 siRNA was purchased from Dharmacon (L-015377-00-0005 ON-TARGETplus siRNA SMARTpool) and was used at a final concentration of 15 nM.

For the rescue experiment (Fig. 6) siRNA#2 was transfected using Lipofectamine RNAiMax 24 h after plating cells in the imaging chamber slide. Endogenous FADD knockdown was rescued by the addition of doxycycline to induce the expression of FADD transgene 8 h after the knockdown. Imaging was initiated 24 h after the knockdown.

Lentiviral constructs and transduction

Stable cells expressing PIP-FUCCI, $FADD_{WT}$, $FADD_{Dbox}$, and $FADD_{KEN}$ were produced by Lentivirus transduction. Lentiviruses were prepared by transfecting HEK 293FT cells with pLenti constructs (6 μg), pMD2.G (0.8 μg), and pSPAX2 (4 μg) constructs (pMD2.G and pSPAX2 were a gift from Didier Trono, Addgene plasmids #12259 and #12260). Cell culture medium was changed 24 h post-transfection and Lentivirus were harvested 48 h post-transfection. NCI-H441, NCI-H1975, MCF-7, and HCC827 cells were infected with 1 ml lentivirus particles mixed with 1 ml culture medium in 6-well dish overnight. The following day, the infection medium was removed and replaced with a complete medium containing 500 ug/ml Neomycin (G418) (PIP-FUCCI stable expression) or puromycin 10 ug/ml to select $FADD_{WT}$, $FADD_{Dbox}$, $FADD_{KEN}$, $FADD_{S194A}$, and $FADD_{S194D}$ transduced cells. Total cell lysates were subjected to Western blot analysis to confirm the protein expression as described above. Single-cell clones were obtained by serial dilution in 96-well plates followed by outgrowth into larger dishes.

Transfections and immunoprecipitation

Transfection of HEK 293FT cells was achieved using the standard Calcium phosphate transfection method (Calcium Phosphate Transfection Kit, Invitrogen K2780-01) using the manufacturer guidelines. The culture medium was changed 24 h after transfection and cells were harvested 48 h post-transfection. The cells cultured on 100 mm tissue culture dishes were rinsed with PBS and then scraped into a lysis buffer containing 50 mM HEPES pH 7.4, 10 mM EDTA, 150 mM NaCl, 1% NP-40, DOC 0.5%, SDS 0.1% with freshly added protease and phosphatase inhibitor cocktail (Roche). The supernatant was collected after centrifugation at 16,800*g* for 10 min at 4 °C. For immunoblotting, lysates were boiled in 2X Laemmli buffer, and proteins were resolved by SDS-PAGE using 4 to 20% Mini-PROTEAN TGX Precast Gels (Bio-rad #4561093EDU). The proteins were transferred onto PVDF using Bio-rad *Trans*-Blot Turbo Transfer System (1704150EDU) and immunoblotted with the indicated antibodies. Immunocomplexes were visualized using the Bio-rad Clarity Western ECL Substrate Chemiluminescent HRP substrate (Bio-rad 1705061). For immunoprecipitation (myc IP), protein concentration was measured using DC protein assay reagent (BioRad), and an equal amount of protein was added to respective beads (ChromoTek myc-Trap beads). Beads were incubated with lysates for 1 h at 4 °C on a rotator, washed three times with lysis buffer, followed by resuspension in 2X Laemmli buffer and loaded on SDS polyacrylamide gels for Western blot analysis. Immune complexes were split into two aliquots (90% and 10%) which were run separately on SDS-PAGE gels and transferred to PVDF membranes. The membranes with 90% of immune complexes were blotted for GST FADD whereas those with 10% of immune complexes were blotted for myc-Cdh1. For Cdc27 IP (Fig. 4*F*) and Halo IP (Fig. S7*E*), protein concentration was measured using a DC protein assay reagent (BioRad). An equal amount of protein (0.5ug) was incubated with either Cdc27 Antibodies (CDC27 IP, Fig. 4*F*) or Halo nanobodies conjugated Sepharose beads (reverse IP, Fig. S7*F*) at 4 °C on a rotator for 3 h followed by addition of Pierce Protein G magnetic beads (Thermo Fisher Catalog #88847) to the CDC27 IP. Beads were incubated with lysates for 1 h at 4 °C on a rotator, washed three times with lysis buffer, followed by resuspension in 2X Laemmli buffer and loaded on SDS polyacrylamide gels for Western blot analysis.

Immunocytochemistry

Immunocytochemistry assays were performed using fixed cells on round cover glass, #1.5 thickness, 10 mm (Thomas Scientific, 1217N78). NCI-H441 cells were grown on the coverslips and fixed for 10 min with 3.7% paraformaldehyde and quenched with 10 mM ammonium chloride. Cells were then permeabilized with 0.1% Triton X-100 in PBS for 10 min. The coverslips were then washed with PBS and blocked in 1XPBS, 2.5% goat serum (Sigma), 0.2% Tween 20 for 10 min followed by 10 min blocking in PBS, 0.4% fish skin gelatin (Sigma), and 0.2% Tween 20. Cells were incubated with primary antibodies for 1 h at room temperature. The coverslips were then washed with PBS, 0.2% Tween 20, and incubated with Alexa Fluor 594 or 647 secondary antibodies for 45 min, washed as described above, and mounted on glass slides in ProLong Diamond Antifade Mountant (Thermo Fisher Scientific-P36965). IF imaging involving fixed cell imaging was

treated with Janelia Fluor 646 HaloTag Ligand (Promega catalogue # GA1120) according to manufacturer's guidelines.

Live cell imaging

NCI-H441, NCI-H1975, and HCC827 cells were plated 16 h before the siRNA transfection, in either CELLVIS 12 well #1.5 glass bottom dishes (CELLVIS, P121.5HN) or 8-well multi-chamber #1.5 glass bottom slides (LABTKII, 155409). Cells were plated at a confluence such that the density would remain sub-confluent until the end of the imaging period. Live cell imaging was performed 24 h post knockdown in phenol red–free RPMI supplemented with 10% FBS and antibiotics (penicillin-streptomycin). Cells were imaged in a humidified chamber that maintains 5% CO2 and 37 °C temperature. Images were taken in GFP and mCherry channels every 10 min on a Zeiss LSM800 Axio Observer.Z1/7 confocal microscope using plan-Apochromat 10X/0.45 M27 objective. The total time exposure was kept under 400 ms for each timepoint to avoid photobleaching and phototoxicity. Images were processed using custom ImageJ macro and custom MATLAB scripts as described below.

Image processing

The images acquired during live cell imaging were pre-processed to remove the background using a Gaussian filter in image J. Where the nuclear channel is absent, a maxima of mVenus and mCherry is used to track cells using trackmate (49). Tracks information and intensities of each channel are then provided to custom MATLAB scripts to produce intensity *versus* time graphs. Representative data from at least three different experiments each with a minimum of 100 cells is shown. ImageJ macro and MATLAB scripts with instructions are uploaded to Github and are available upon request.

In vitro *APC/C-Cdh1 E3-ligase assay*

APC-Cdh1 activity assays (as described in (11)) were used to evaluate the difference in E3 ligase activity of immuno-purified APC/C-Cdh1 derived from control siRNA transfected cells and FADD siRNA transfected cells. Briefly, anti-CDC27 antibody coupled protein A/G magnetic Dynabeads were incubated with equal concentrations of extracts from late G1 phase cells (3 h post-nocodazole release). Beads were washed with buffer (25 mM HEPES, pH7.5, 1.5 mM $MgCl_2$, 5 mM KCl) and used as a source of APC/C-Cdh1. For ubiquitination assays, 4 µl bead slurry was used in 10 µl reactions containing purified E1, E2 (UBE2C and UBE2S), ubiquitin, energy mix (10 mM phosphocreatine, 0.5 mM ATP and 50ug/ul creatine phosphokinase) and substrate (His-myc-Cyclin B_{1-102}) for 0 to 30 min. Samples were western blotted for cyclin B1.

Statistical analysis

Graphpad PRISM 8 was used to perform statistical analysis. Statistical significance was measured using a 2-tailed unpaired student *t* test with Welch's correction. *p* values are reported in the graphs and explained in the figure legends. $^{*}p < 0.05$; $^{**}p < 0.01$; and $^{***}p < 0.001$. n.s. denotes not significant.

Data availability

Source Data and Supplementary Data for the figures will be made available from the corresponding authors upon request.

Code availability

The pre-processing codes before running Trackmate in ImageJ analysis and the MATLAB codes for the analysis of Fiji generated data are deposited at Github (https://github.com/sahezeel/PIP-FUCCI-Analysis-codes). Additional modified scripts are available from the corresponding authors upon reasonable request.

Supporting information—This article contains supporting information.

Acknowledgments—We thank Anupama Pal, Heli Patel, Grant Young, Drew Calcaterra, Grayson Rice, Julianne Thomas and Maya Mileski for their valuable help in preparing reagents and for performing ancillary experiments. Thanks to Steven Kronenberg for his help in graphics design. We would like to thank the University of Michigan FACS core facility and University of Michigan Microscopy core facility for their help in acquisition of data. Special thanks to Eric Rentchler and Aaron Taylor of the University of Michigan Microscopy core for their help in writing Trackmate codes and MATLAB codes.

Author contributions—S. A. and A. R. conceptualization; S. A., M. S., W. J., Y. L., R. D., S. D. C., and A. R. methodology; S. A., S. R., R. D., C. J. G., and S. D. C. software; S. A., M. S., S. R., W. J., Y. L., R. D., C. J. G., and S. D. C. validation; S. A., M. S., S. R., W. J., Y. L., R. D., and S. D. C. investigation; S. A., M. S., S. R., W. J., Y. L., R. D., and S. D. C. formal analysis; S. A. and A. R. data curation; S. A., S. D. C., and A. R. visualization; S. A., D. R., T. S. L., C. J. G., S. D. C., and A. R. supervision; S. A. and A. R. writing–original draft; S. A., D. R., T. S. L., C. J. G., S. D. C., and A. R. writing–review and editing; T. S. L., C. J. G., S. D. C., and A. R. project administration; T. S. L. and A. R. funding acquisition; A. R. resources.

Funding and additional information—Each of the cores used for the research is funded through the University of Michigan Rogel Cancer Center and the National Cancer Institute grant P30 CA046592. A. R. is supported by funds from NIH grant R01CA241764, U01CA216449 and Department of Defense grant HT94252310210. T. S. L. is funded through U01CA216449. The content is solely the responsibility of the authors and does not necessarily represent the official views of the National Institutes of Health.

Conflict of interests—The authors declare that no actual, potential, or perceived conflict of interest or competing interests exists in relation to this research.

Abbreviations—The abbreviations used are: CTRL, control siRNA-treated cells; Emi1, early mitotic inhibitor 1; FADD, Fas-associated protein with death domain; FBS, fetal bovine serum; MEF, mouse embryonic fibroblasts; Rb, retinoblastoma protein.

References

1. Narasimha, A. M., Kaulich, M., Shapiro, G. S., Choi, Y. J., Sicinski, P., and Dowdy, S. F. (2014) Cyclin D activates the Rb tumor suppressor by mono-phosphorylation. *Elife* **3**, e02872
2. Yao, G., Lee, T. J., Mori, S., Nevins, J. R., and You, L. (2008) A bistable Rb-E2F switch underlies the restriction point. *Nat. Cell Biol.* **10**, 476–482
3. Cappell, S. D., Chung, M., Jaimovich, A., Spencer, S. L., and Meyer, T. (2016) Irreversible APC(Cdh1) inactivation underlies the point of no return for cell-cycle entry. *Cell* **166**, 167–180
4. Robbins, J. A., and Cross, F. R. (2010) Requirements and reasons for effective inhibition of the anaphase promoting complex activator CDH1. *Mol. Biol. Cell* **21**, 914–925
5. Malumbres, M., and Barbacid, M. (2009) Cell cycle, CDKs and cancer: a changing paradigm. *Nat. Rev. Cancer* **9**, 153–166
6. Nakayama, K. I., and Nakayama, K. (2006) Ubiquitin ligases: cell-cycle control and cancer. *Nat. Rev. Cancer* **6**, 369–381
7. Peters, J. M. (2006) The anaphase promoting complex/cyclosome: a machine designed to destroy. *Nat. Rev. Mol. Cell Biol.* **7**, 644–656
8. Pines, J. (2011) Cubism and the cell cycle: the many faces of the APC/C. *Nat. Rev. Mol. Cell Biol.* **12**, 427–438
9. Watson, E. R., Brown, N. G., Peters, J. M., Stark, H., and Schulman, B. A. (2019) Posing the APC/C E3 ubiquitin ligase to orchestrate cell division. *Trends Cell Biol.* **29**, 117–134
10. Bassermann, F., Eichner, R., and Pagano, M. (2014) The ubiquitin proteasome system - implications for cell cycle control and the targeted treatment of cancer. *Biochim. Biophys. Acta* **1843**, 150–162
11. Cappell, S. D., Mark, K. G., Garbett, D., Pack, L. R., Rape, M., and Meyer, T. (2018) EMI1 switches from being a substrate to an inhibitor of APC/C(CDH1) to start the cell cycle. *Nature* **558**, 313–317
12. Frye, J. J., Brown, N. G., Petzold, G., Watson, E. R., Grace, C. R., Nourse, A., *et al.* (2013) Electron microscopy structure of human APC/C(CDH1)-EMI1 reveals multimodal mechanism of E3 ligase shutdown. *Nat. Struct. Mol. Biol.* **20**, 827–835
13. Hwang, H. C., and Clurman, B. E. (2005) Cyclin E in normal and neoplastic cell cycles. *Oncogene* **24**, 2776–2786
14. Miller, J. J., Summers, M. K., Hansen, D. V., Nachury, M. V., Lehman, N. L., Loktev, A., *et al.* (2006) Emi1 stably binds and inhibits the anaphase-promoting complex/cyclosome as a pseudosubstrate inhibitor. *Genes Dev.* **20**, 2410–2420
15. Wang, W., and Kirschner, M. W. (2013) Emi1 preferentially inhibits ubiquitin chain elongation by the anaphase-promoting complex. *Nat. Cell Biol.* **15**, 797–806
16. Yamano, H. (2013) EMI1, a three-in-one ubiquitylation inhibitor. *Nat. Struct. Mol. Biol.* **20**, 773–774
17. Chinnaiyan, A. M., O'Rourke, K., Tewari, M., and Dixit, V. M. (1995) FADD, a novel death domain-containing protein, interacts with the death domain of Fas and initiates apoptosis. *Cell* **81**, 505–512
18. Chinnaiyan, A. M., Tepper, C. G., Seldin, M. F., O'Rourke, K., Kischkel, F. C., Hellbardt, S., *et al.* (1996) FADD/MORT1 is a common mediator of CD95 (Fas/APO-1) and tumor necrosis factor receptor-induced apoptosis. *J. Biol. Chem.* **271**, 4961–4965
19. Zhang, J., and Winoto, A. (1996) A mouse Fas-associated protein with homology to the human Mort1/FADD protein is essential for Fas-induced apoptosis. *Mol. Cell. Biol.* **16**, 2756–2763
20. Alappat, E. C., Feig, C., Boyerinas, B., Volkland, J., Samuels, M., Murmann, A. E., *et al.* (2005) Phosphorylation of FADD at serine 194 by CKIalpha regulates its nonapoptotic activities. *Mol. Cell* **19**, 321–332
21. Chen, G., Bhojani, M. S., Heaford, A. C., Chang, D. C., Laxman, B., Thomas, D. G., *et al.* (2005) Phosphorylated FADD induces NF-kappaB, perturbs cell cycle, and is associated with poor outcome in lung adenocarcinomas. *Proc. Natl. Acad. Sci. U. S. A.* **102**, 12507–12512
22. Bowman, B. M., Sebolt, K. A., Hoff, B. A., Boes, J. L., Daniels, D. L., Heist, K. A., *et al.* (2015) Phosphorylation of FADD by the kinase CK1alpha promotes KRASG12D-induced lung cancer. *Sci. Signal.* **8**, ra9
23. Bhojani, M. S., Chen, G., Ross, B. D., Beer, D. G., and Rehemtulla, A. (2005) Nuclear localized phosphorylated FADD induces cell proliferation and is associated with aggressive lung cancer. *Cell Cycle* **4**, 1478–1481
24. Gibcus, J. H., Menkema, L., Mastik, M. F., Hermsen, M. A., de Bock, G. H., van Velthuysen, M. L., *et al.* (2007) Amplicon mapping and expression profiling identify the Fas-associated death domain gene as a new driver in the 11q13.3 amplicon in laryngeal/pharyngeal cancer. *Clin. Cancer Res.* **13**, 6257–6266
25. Drakos, E., Leventaki, V., Atsaves, V., Schlette, E. J., Lin, P., Vega, F., *et al.* (2011) Expression of serine 194-phosphorylated Fas-associated death domain protein correlates with proliferation in B-cell non-Hodgkin lymphomas. *Hum. Pathol.* **42**, 1117–1124
26. Prapinjumrune, C., Morita, K., Kuribayashi, Y., Hanabata, Y., Shi, Q., Nakajima, Y., *et al.* (2010) DNA amplification and expression of FADD in oral squamous cell carcinoma. *J. Oral Pathol. Med.* **39**, 525–532
27. Pfleger, C. M., and Kirschner, M. W. (2000) The KEN box: an APC recognition signal distinct from the D box targeted by Cdh1. *Genes Dev.* **14**, 655–665
28. Grant, G. D., Kedziora, K. M., Limas, J. C., Cook, J. G., and Purvis, J. E. (2018) Accurate delineation of cell cycle phase transitions in living cells with PIP-FUCCI. *Cell Cycle* **17**, 2496–2516
29. Gazdar, A. F., Carney, D. N., Nau, M. M., and Minna, J. D. (1985) Characterization of variant subclasses of cell lines derived from small cell lung cancer having distinctive biochemical, morphological, and growth properties. *Cancer Res.* **45**, 2924–2930
30. Phelps, R. M., Johnson, B. E., Ihde, D. C., Gazdar, A. F., Carbone, D. P., McClintock, P. R., *et al.* (1996) NCI-navy medical oncology branch cell line data base. *J. Cell. Biochem. Suppl.* **24**, 32–91
31. Virmani, A. K., Fong, K. M., Kodagoda, D., McIntire, D., Hung, J., Tonk, V., *et al.* (1998) Allelotyping demonstrates common and distinct patterns of chromosomal loss in human lung cancer types. *Genes Chromosomes Cancer* **21**, 308–319
32. Dhillon, A. S., Hagan, S., Rath, O., and Kolch, W. (2007) MAP kinase signalling pathways in cancer. *Oncogene* **26**, 3279–3290
33. Di Fiore, B., and Pines, J. (2007) Emi1 is needed to couple DNA replication with mitosis but does not regulate activation of the mitotic APC/C. *J. Cell Biol.* **177**, 425–437
34. Sakaue-Sawano, A., Kurokawa, H., Morimura, T., Hanyu, A., Hama, H., Osawa, H., *et al.* (2008) Visualizing spatiotemporal dynamics of multicellular cell-cycle progression. *Cell* **132**, 487–498
35. Meyer, H. J., and Rape, M. (2014) Enhanced protein degradation by branched ubiquitin chains. *Cell* **157**, 910–921
36. Spencer, S. L., Cappell, S. D., Tsai, F. C., Overton, K. W., Wang, C. L., and Meyer, T. (2013) The proliferation-quiescence decision is controlled by a bifurcation in CDK2 activity at mitotic exit. *Cell* **155**, 369–383
37. Kabra, N. H., Kang, C., Hsing, L. C., Zhang, J., and Winoto, A. (2001) T cell-specific FADD-deficient mice: FADD is required for early T cell development. *Proc. Natl. Acad. Sci. U. S. A.* **98**, 6307–6312
38. Zhang, J., Cado, D., Chen, A., Kabra, N. H., and Winoto, A. (1998) Fas-mediated apoptosis and activation-induced T-cell proliferation are defective in mice lacking FADD/Mort1. *Nature* **392**, 296–300
39. Baykara, O., Dalay, N., Bakir, B., Bulut, P., Kaynak, K., and Buyru, N. (2017) The EMSY gene collaborates with CCND1 in non-small cell lung carcinogenesis. *Int. J. Med. Sci.* **14**, 675–679
40. Gupta, V. K., Feber, A., Xi, L., Pennathur, A., Wu, M., Luketich, J. D., *et al.* (2008) Association between CCND1 G/A870 polymorphism, allele-specific amplification, cyclin D1 expression, and survival in esophageal and lung carcinoma. *Clin. Cancer Res.* **14**, 7804–7812
41. Ragin, C. C., Taioli, E., Weissfeld, J. L., White, J. S., Rossie, K. M., Modugno, F., *et al.* (2006) 11q13 amplification status and human papillomavirus in relation to p16 expression defines two distinct etiologies of head and neck tumours. *Br. J. Cancer* **95**, 1432–1438
42. Ramos-Garcia, P., Ruiz-Avila, I., Gil-Montoya, J. A., Ayen, A., Gonzalez-Ruiz, L., Navarro-Trivino, F. J., *et al.* (2017) Relevance of chromosomal band 11q13 in oral carcinogenesis: an update of current knowledge. *Oral Oncol.* **72**, 7–16
43. Alappat, E. C., Volkland, J., and Peter, M. E. (2003) Cell cycle effects by C-FADD depend on its C-terminal phosphorylation site. *J. Biol. Chem.* **278**, 41585–41588

44. Matsuyoshi, S., Shimada, K., Nakamura, M., Ishida, E., and Konishi, N. (2006) FADD phosphorylation is critical for cell cycle regulation in breast cancer cells. *Br. J. Cancer* **94**, 532–539
45. Osborn, S. L., Sohn, S. J., and Winoto, A. (2007) Constitutive phosphorylation mutation in Fas-associated death domain (FADD) results in early cell cycle defects. *J. Biol. Chem.* **282**, 22786–22792
46. Choi, E., Dial, J. M., Jeong, D. E., and Hall, M. C. (2008) Unique D box and KEN box sequences limit ubiquitination of Acm1 and promote pseudosubstrate inhibition of the anaphase-promoting complex. *J. Biol. Chem.* **283**, 23701–23710
47. Yuan, X., Srividhya, J., De Luca, T., Lee, J. H., and Pomerening, J. R. (2014) Uncovering the role of APC-Cdh1 in generating the dynamics of S-phase onset. *Mol. Biol. Cell* **25**, 441–456
48. Li, M., Shin, Y. H., Hou, L., Huang, X., Wei, Z., Klann, E., *et al.* (2008) The adaptor protein of the anaphase promoting complex Cdh1 is essential in maintaining replicative lifespan and in learning and memory. *Nat. Cell Biol.* **10**, 1083–1089
49. Tinevez, J. Y., Perry, N., Schindelin, J., Hoopes, G. M., Reynolds, G. D., Laplantine, E., *et al.* (2017) TrackMate: an open and extensible platform for single-particle tracking. *Methods* **115**, 80–90